Transfer Function of the LARES Retroreflector Array

By
David A. Arnold
94 Pierce Rd
Watertown, MA 02472
617-924-6812
david-arnold@earthlink.net
Smithsonian Astrophysical Observatory (Retired)

Abstract

This paper presents the final transfer function of the LARES retroreflector array. The report is patterned after the 1979 LAGEOS report and contains the same kind of analyses with the exception of the infrared transfer function since LARES has no infrared cube corners.

Table of Contents

1. Introduction

.Although the design of LARES is partly derived from that of LAGEOS there are many differences: the orbit [1-7], the optical design [8-10], the material used[11-13], the single piece design [1,14-16]. Briefly, since the radius of LARES is 18.2 cm and the radius of LAGEOS is 30 cm there are fewer cube corners. This results in more variation in the transfer function with incidence angle on the satellite. However, the smaller radius of the satellite reduces the spread in range between the active cube corners. As with LAGEOS the orientation of each cube corner in its holder is varied to avoid anomalous effects due to loss of total internal reflection at certain incidence angles.

2. Cube corner specifications

The cube corners on LARES have a circular entrance face 1.5 inches (3.81cm) in diameter which gives an aperture of 11.4009 sq cm. The length from vertex to face is 1.096 inches (2.7838 cm). The dihedral angles of CCRs (fused silica Supralis 311) have to be between (90 degrees + 1.5 arcsec) + 0.5 arcsec and (90 degrees + 1.5 arcsec) -0.5 arcsec.
Surface properties: assuming a reference wavelength of 532 nm, the tolerances on all optical surfaces are 1/10th wavelength, except for the entrance face, which is 1/8th wavelength. The exiting wavefront tolerance is 1/4th wavelength. All tolerances are peak to valley (not rms).

The phase index of refraction of the fused silica is 1.461 at 532 nm. The group index of refraction is 1.484. The group index of refraction has been used in the computations since the range correction depends on the group index of refraction.

The actual dihedral angle offsets for each cube corner are listed in the table below.

N = Northern hemisphere
S = Southern hemisphere
The roman numerals are the row number

Cavity ID	A2-A1	A3-A4	A2-A4
N-I1	1.46	1.57	1.65
N-II1	1.63	1.64	1.52
N-II2	1.58	1.73	1.59
N-II3	1.54	1.41	1.6
N-II4	1.56	1.75	1.8
N-II5	1.55	1.52	1.56
N-III1	1.60	1.46	1.63
N-III2	1.42	1.22	1.59
N-III3	1.63	1.65	1.54
N-III4	1.61	1.72	1.63
N-III5	1.83	1.57	1.59
N-III6	1.67	1.73	1.89
N-III7	1.5	1.5	1.52
N-III8	1.47	1.69	1.95
N-III9	1.55	1.66	1.67
N-III10	1.42	1.19	1.37
N-IV1	1.41	1.78	1.44
N-IV2	1.82	1.74	1.79
N-IV3	1.78	1.51	1.64
N-IV4	1.45	1.19	1.77
N-IV5	1.73	1.56	1.15
N-IV6	1.72	1.75	1.87
N-IV7	1.33	1.35	1.35
N-IV8	1.34	1.22	1.38
N-IV9	1.47	1.27	1.48
N-IV10	1.63	1.49	1.79
N-IV11	1.5	1.51	1.61
N-IV12	1.56	1.55	1.54

N-IV13	1.89	1.34	1.5
N-IV14	1.72	1.8	1.53
N-V1	1.95	1.66	1.74
N-V2	1.6	1.55	1.61
N-V3	1.62	1.46	1.67
N-V4	1.54	1.89	1.45
N-V5	1.5	1.71	1.84
N-V6	1.44	1.53	1.50
N-V7	1.73	1.89	1.8
N-V8	1.52	1.86	1.8
N-V9	1.57	1.56	1.56
N-V10	1.65	1.54	1.4
N-V11	1.55	1.49	1.67
N-V12	1.81	1.4	1.42
N-V13	1.39	1.37	1.46
N-V14	1.6	1.43	1.94
N-V15	1.82	1.81	1.75
N-V16	1.63	1.81	1.52
S-I1	1.32	1.41	1.29
S-II1	1.71	1.84	1.59
S-II2	1.81	1.91	1.73
S-II3	1.82	1.84	1.91
S-II4	1.68	1.62	1.76
S-II5	1.56	1.62	1.57
S-III1	1.34	1.16	1.33
S-III2	1.7	1.56	1.49
S-III3	1.78	1.51	1.94
S-III4	1.53	1.65	1.42
S-III5	1.61	1.59	1.84
S-III6	1.27	1.57	1.39
S-III7	1.64	1.59	1.52
S-III8	1.88	1.6	1.82
S-III9	1.37	1.46	1.98
S-III10	1.09	1.54	1.18
S-IV1	1.61	1.53	1.62
S-IV2	1.79	1.89	1.50
S-IV3	1.45	1.9	1.83
S-IV4	1.29	1.77	1.33
S-IV5	1.72	1.44	1.51
S-IV6	1.66	1.55	1.66
S-IV7	1.55	1.58	1.61
S-IV8	1.83	1.56	1.13
S-IV9	1.51	1.52	1.36
S-IV10	1.5	1.62	1.69
S-IV11	1.58	1.59	1.83
S-IV12	1.08	1.67	1.31
S-IV13	1.48	1.55	1.54
S-IV14	1.52	1.44	1.57
S-V1	1.76	1.32	1.6
S-V2	1.02	1.28	1.76
S-V3	1.84	1.61	1.88
S-V4	1.43	1.62	1.83
S-V5	1.68	1.90	1.76
S-V6	1.6	1.53	1.54
S-V7	1.48	1.72	1.61
S-V8	1.51	1.6	1.99

S-V9	1.32	1.37	1.32
S-V10	1.56	1.56	1.51
S-V11	1.47	1.2	1.69
S-V12	1.58	1.43	1.56
S-V13	1.61	1.68	1.57
S-V14	1.81	1.86	1.56
S-V15	1.54	1.89	1.65
S-V16	1.43	1.35	1.45

Table 2.1. Dihedral angle offsets (arcsec) for each cube in the array.

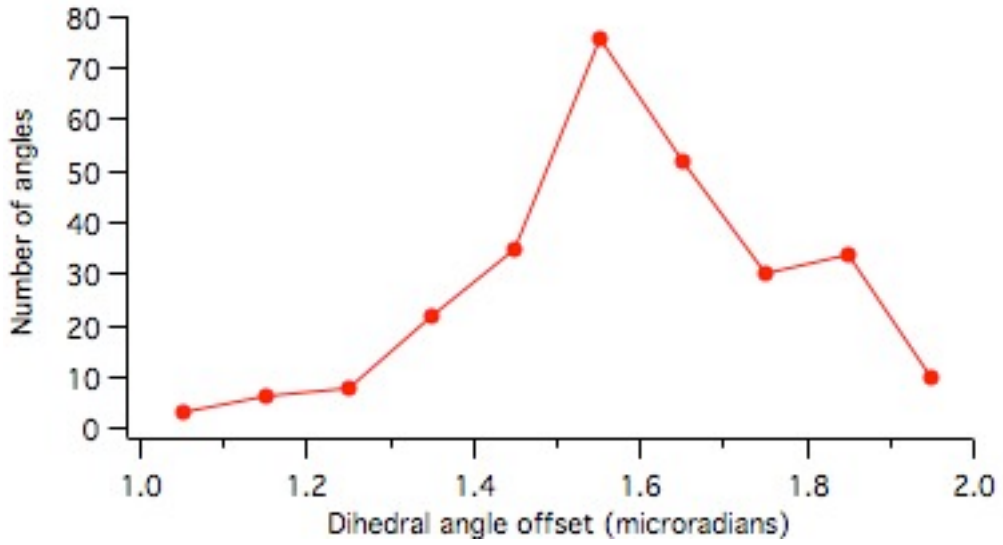

Figure 2.1. Distribution of the dihedral angle offsets (.1 arcsec bins). The average offset is 1.58 arcsec which is close to the nominal 1.50 arcsec offset. There are 92 cubes with three angles each for a total of 276 angles.

3. Geometry of the array

The satellite has two hemispheres. Each hemisphere has a pole cube and 4 rings of cubes containing 5, 10, 14, and 16 cubes. The rings are at latitude 10, 30, 50, and 70 degrees. There are 4 bolt holes along the equator for handling the satellite. The radius of the satellite is 182 mm. The center of the front face of the cube corners is recessed 3.5 millimeters below the surface of the satellite. The distance from the front face to the center of the satellite is 182 – 3.5 = 178.5 millimeters. The data in sections 3.1, 3.2, and 3.3 were provided by Scuola di Ingegneria Aerospaziale and DIAEE of Sapienza University that was in charge of the design.. The data in section 3.4 is computed from this data.

3.1 Rotation angle of each cube corner in its holder

Starting from the polar cavity, the first cavity of each row has to rotate 23° with respect to its longitudinal axis and with respect to the first cavity of the previous row. On each

row, each CCR, moving clockwise from the first one, have to rotate 23 deg with respect to the previous one. On row V (and -V) the first cavity have to rotate 45° from the horizontal plane, for mechanical reasons, then the following CCRs are rotated by the sequence +90°, +30°, 90°, +30°, and so on. The table shows the absolute value of the rotation angle for each cavity, starting from the polar taken as reference cavity for the orientation. The southern hemisphere is a mirror image of the northern hemisphere.

CCR # in row→	1	2	3	4	5	6	7	8	9	10	11	12	13	14	15	16
Row↓																
I	0															
II	23	46	69	92	115											
III	46	69	92	115	138	161	184	207	230	253						
IV	69	92	115	138	161	184	207	230	253	276	299	322	345	8		
V	45	135	165	255	285	15	45	135	165	255	285	15	45	135	165	255
-V	45	135	165	255	285	15	45	135	165	255	285	15	45	135	165	255
-IV	69	92	115	138	161	184	207	230	253	276	299	322	345	8		
-III	46	69	92	115	138	161	184	207	230	253						
-II	23	46	69	92	115											
-I	0															

Table 3.1. Orientation of each cube corner in its holder. The orientations are varied in order to eliminate anomalous effects due to loss of total internal reflection.

3.2 Latitude and Longitude of each cube corner

The first two columns are the latitude and increment between cube corners
Col 1-16 = Longitude (clockwise)

		1	2	3	4	5	6	7	8	9	10	11	12	13	14	15	16
90																	
70	72	0	72	144	216	288											
50	36	23	59	95	131	167	203	239	275	311	347						
30	25.71	0	25.71	51.42	77.13	102.84	128.55	154.26	179.97	205.68	231.39	257.1	282.81	308.52	334.2		
10	22.5	11.25	33.75	56.25	78.75	101.25	123.75	146.25	168.75	191.25	213.75	236.25	258.75	281.25	303.8	326.25	348.8
-10	22.5	11.25	33.75	56.25	78.75	101.25	123.75	146.25	168.75	191.25	213.75	236.25	258.75	281.25	303.8	326.25	348.8
-30	25.71	0	25.71	51.42	77.13	102.84	128.55	154.26	179.97	205.68	231.39	257.1	282.81	308.52	334.2		
-50	36	23	59	95	131	167	203	239	275	311	347						
-70	72	0	72	144	216	288											
-90																	

Table 3.2. Longitude and latitude of each cube corner.

3.3 Position of each cube corner

Z is the polar axis, X and Y are in the equatorial plane with X in the direction of one of the four hemispherical cavities. In this reference frame the intersection of the CCR cavities with the spherical surface in mm is reported in the following table. Note that the roman numerals represents the rows and the Arabic numeral the CCR number in the row. In the following table are reported the coordinates of CCR in one hemisphere.

		X	**Y**	**Z**
1	I-1	0.00	0.00	182.00
2	II-1	62.25	0.00	171.02
3	II-2	19.24	59.20	171.02
4	II-3	-50.36	36.59	171.02
5	II-4	-50.36	-36.59	171.02

6	II-5	19.24	-59.20	171.02
7	III-1	107.69	45.71	139.42
8	III-2	60.25	100.28	139.42
9	III-3	-10.20	116.54	139.42
10	III-4	-76.75	88.29	139.42
11	III-5	-113.99	26.32	139.42
12	III-6	-107.69	-45.71	139.42
13	III-7	-60.25	-100.28	139.42
14	III-8	10.20	-116.54	139.42
15	III-9	76.75	-88.29	139.42
16	III-10	113.99	-26.32	139.42
17	IV-1	157.62	0.00	91.00
18	IV-2	142.01	68.39	91.00
19	IV-3	98.27	123.23	91.00
20	IV-4	35.07	153.66	91.00
21	IV-5	-35.07	153.66	91.00
22	IV-6	-98.27	123.23	91.00
23	IV-7	-142.01	68.39	91.00
24	IV-8	-157.62	0.00	91.00
25	IV-9	-142.01	-68.39	91.00
26	IV-10	-98.27	-123.23	91.00
27	IV-11	-35.07	-153.66	91.00
28	IV-12	35.07	-153.66	91.00
29	IV-13	98.27	-123.23	91.00
30	IV-14	142.01	-68.39	91.00
31	V-1	175.79	34.97	31.60
32	V-2	149.03	99.58	31.60
33	V-3	99.58	149.03	31.60
34	V-4	34.97	175.79	31.60
35	V-5	-34.97	175.79	31.60
36	V-6	-99.58	149.03	31.60
37	V-7	-149.03	99.58	31.60
38	V-8	-175.79	34.97	31.60
39	V-9	-175.79	-34.97	31.60
40	V-10	-149.03	-99.58	31.60
41	V-11	-99.58	-149.03	31.60
42	V-12	-34.97	-175.79	31.60
43	V-13	34.97	-175.79	31.60
44	V-14	99.58	-149.03	31.60
45	V-15	149.03	-99.58	31.60
46	V-16	175.79	-34.97	31.60

Table 3.3. Position of each cube corner in the array.

3.4 Data file used for the simulations

In the table below the positions are in meters and the angles are in degrees. The angle Alpha is the rotation angle of the cube in its holder. This is the negative of the angles

given in section 3.1 since the direction of the angle is defined differently. The positions in section 3.3 are on the surface of the sphere. The data in the table below is for the center of the front face of each cube corner which is recessed 3.5 mm below the surface.

Cap	Row	Unit	X	Y	Z	Longitude	Colatitude	Alpha
1	1	1	0.00000	0.00000	0.17850	0.000	0.000	0.000
1	2	1	0.06105	0.00000	0.16774	0.000	20.000	-23.000
1	2	2	0.01887	0.05806	0.16774	72.000	20.000	-46.000
1	2	3	-0.04939	0.03588	0.16774	144.000	20.000	-69.000
1	2	4	-0.04939	-0.03588	0.16774	216.000	20.000	-92.000
1	2	5	0.01887	-0.05806	0.16774	288.000	20.000	-115.000
1	3	1	0.10562	0.04483	0.13674	23.000	40.000	-46.000
1	3	2	0.05909	0.09835	0.13674	59.000	40.000	-69.000
1	3	3	-0.01000	0.11430	0.13674	95.000	40.000	-92.000
1	3	4	-0.07527	0.08659	0.13674	131.000	40.000	-115.000
1	3	5	-0.11180	0.02581	0.13674	167.000	40.000	-138.000
1	3	6	-0.10562	-0.04483	0.13674	203.000	40.000	-161.000
1	3	7	-0.05909	-0.09835	0.13674	239.000	40.000	-184.000
1	3	8	0.01000	-0.11430	0.13674	275.000	40.000	-207.000
1	3	9	0.07527	-0.08659	0.13674	311.000	40.000	-230.000
1	3	10	0.11180	-0.02581	0.13674	347.000	40.000	-253.000
1	4	1	0.15459	0.00000	0.08925	0.000	60.000	-69.000
1	4	2	0.13928	0.06707	0.08925	25.714	60.000	-92.000
1	4	3	0.09638	0.12086	0.08925	51.429	60.000	-115.000
1	4	4	0.03440	0.15071	0.08925	77.143	60.000	-138.000
1	4	5	-0.03440	0.15071	0.08925	102.857	60.000	-161.000
1	4	6	-0.09638	0.12086	0.08925	128.571	60.000	-184.000
1	4	7	-0.13928	0.06707	0.08925	154.286	60.000	-207.000
1	4	8	-0.15459	0.00000	0.08925	180.000	60.000	-230.000
1	4	9	-0.13928	-0.06707	0.08925	205.714	60.000	-253.000
1	4	10	-0.09638	-0.12086	0.08925	231.429	60.000	-276.000
1	4	11	-0.03440	-0.15071	0.08925	257.143	60.000	-299.000
1	4	12	0.03440	-0.15071	0.08925	282.857	60.000	-322.000
1	4	13	0.09638	-0.12086	0.08925	308.571	60.000	-345.000
1	4	14	0.13928	-0.06707	0.08925	334.286	60.000	-8.000
1	5	1	0.17241	0.03429	0.03100	11.250	80.000	-45.000
1	5	2	0.14616	0.09766	0.03100	33.750	80.000	-135.000
1	5	3	0.09766	0.14616	0.03100	56.250	80.000	-165.000
1	5	4	0.03429	0.17241	0.03100	78.750	80.000	-255.000
1	5	5	-0.03429	0.17241	0.03100	101.250	80.000	-285.000
1	5	6	-0.09766	0.14616	0.03100	123.750	80.000	-15.000
1	5	7	-0.14616	0.09766	0.03100	146.250	80.000	-45.000
1	5	8	-0.17241	0.03429	0.03100	168.750	80.000	-135.000
1	5	9	-0.17241	-0.03429	0.03100	191.250	80.000	-165.000
1	5	10	-0.14616	-0.09766	0.03100	213.750	80.000	-255.000
1	5	11	-0.09766	-0.14616	0.03100	236.250	80.000	-285.000
1	5	12	-0.03429	-0.17241	0.03100	258.750	80.000	-15.000
1	5	13	0.03429	-0.17241	0.03100	281.250	80.000	-45.000
1	5	14	0.09766	-0.14616	0.03100	303.750	80.000	-135.000
1	5	15	0.14616	-0.09766	0.03100	326.250	80.000	-165.000
1	5	16	0.17241	-0.03429	0.03100	348.750	80.000	-255.000
2	6	1	0.17241	0.03429	-0.03100	11.250	100.000	-45.000
2	6	2	0.14616	0.09766	-0.03100	33.750	100.000	-135.000
2	6	3	0.09766	0.14616	-0.03100	56.250	100.000	-165.000
2	6	4	0.03429	0.17241	-0.03100	78.750	100.000	-255.000
2	6	5	-0.03429	0.17241	-0.03100	101.250	100.000	-285.000
2	6	6	-0.09766	0.14616	-0.03100	123.750	100.000	-15.000

2	6	7	-0.14616	0.09766	-0.03100	146.250	100.000	-45.000
2	6	8	-0.17241	0.03429	-0.03100	168.750	100.000	-135.000
2	6	9	-0.17241	-0.03429	-0.03100	191.250	100.000	-165.000
2	6	10	-0.14616	-0.09766	-0.03100	213.750	100.000	-255.000
2	6	11	-0.09766	-0.14616	-0.03100	236.250	100.000	-285.000
2	6	12	-0.03429	-0.17241	-0.03100	258.750	100.000	-15.000
2	6	13	0.03429	-0.17241	-0.03100	281.250	100.000	-45.000
2	6	14	0.09766	-0.14616	-0.03100	303.750	100.000	-135.000
2	6	15	0.14616	-0.09766	-0.03100	326.250	100.000	-165.000
2	6	16	0.17241	-0.03429	-0.03100	348.750	100.000	-255.000
2	7	1	0.15459	0.00000	-0.08925	0.000	120.000	-69.000
2	7	2	0.13928	0.06707	-0.08925	25.714	120.000	-92.000
2	7	3	0.09638	0.12086	-0.08925	51.429	120.000	-115.000
2	7	4	0.03440	0.15071	-0.08925	77.143	120.000	-138.000
2	7	5	-0.03440	0.15071	-0.08925	102.857	120.000	-161.000
2	7	6	-0.09638	0.12086	-0.08925	128.571	120.000	-184.000
2	7	7	-0.13928	0.06707	-0.08925	154.286	120.000	-207.000
2	7	8	-0.15459	0.00000	-0.08925	180.000	120.000	-230.000
2	7	9	-0.13928	-0.06707	-0.08925	205.714	120.000	-253.000
2	7	10	-0.09638	-0.12086	-0.08925	231.429	120.000	-276.000
2	7	11	-0.03440	-0.15071	-0.08925	257.143	120.000	-299.000
2	7	12	0.03440	-0.15071	-0.08925	282.857	120.000	-322.000
2	7	13	0.09638	-0.12086	-0.08925	308.571	120.000	-345.000
2	7	14	0.13928	-0.06707	-0.08925	334.286	120.000	-8.000
2	8	1	0.10562	0.04483	-0.13674	23.000	140.000	-46.000
2	8	2	0.05909	0.09835	-0.13674	59.000	140.000	-69.000
2	8	3	-0.01000	0.11430	-0.13674	95.000	140.000	-92.000
2	8	4	-0.07527	0.08659	-0.13674	131.000	140.000	-115.000
2	8	5	-0.11180	0.02581	-0.13674	167.000	140.000	-138.000
2	8	6	-0.10562	-0.04483	-0.13674	203.000	140.000	-161.000
2	8	7	-0.05909	-0.09835	-0.13674	239.000	140.000	-184.000
2	8	8	0.01000	-0.11430	-0.13674	275.000	140.000	-207.000
2	8	9	0.07527	-0.08659	-0.13674	311.000	140.000	-230.000
2	8	10	0.11180	-0.02581	-0.13674	347.000	140.000	-253.000
2	9	1	0.06105	0.00000	-0.16774	0.000	160.000	-23.000
2	9	2	0.01887	0.05806	-0.16774	72.000	160.000	-46.000
2	9	3	-0.04939	0.03588	-0.16774	144.000	160.000	-69.000
2	9	4	-0.04939	-0.03588	-0.16774	216.000	160.000	-92.000
2	9	5	0.01887	-0.05806	-0.16774	288.000	160.000	-115.000
2	10	1	0.00000	0.00000	-0.17850	0.000	180.000	0.000

Table 3.4. Position (m) and orientation (deg) of each cube corner in the array. This is the data file used as input to the simulation programs.

4. Method of computing the transfer function.

The method of computing the transfer function is described in reference 17, Method of Computing Retroreflector Array Transfer Functions. The programs compute the diffraction pattern of each retroreflector. The diffraction patterns are added to obtain the incoherent cross section matrix. The range correction matrix is computed as the weighted mean position of the signal from the retroreflectors at each point in the far field pattern. There are two primary analysis programs. Program TRANSFR computes the whole cross section and range correction matrices. Program RETURN computes the cross section and range correction at a single point in the far field pattern. This program has the capability

of computing pulse shapes and also the coherent return by assigning random phases to the contribution from each retroreflector. Other types of range correction such the half-maximum point on the leading edge of the pulse can be computed.

The transfer function depends on many variables such as the two incidence angles on the array, the horizontal and vertical components of the velocity aberration, and the polarization of the transmitted beam for uncoated cubes. Since it is not feasible to do simulations for all the possible conditions it is necessary to try to pick representative cases to study.

The output of the simulations can be presented in various ways. For example, the cross section or range correction matrix can be analyzed by computing the average value around circles of increasing radius in the far field pattern. The average value within the velocity aberration annulus between the minimum and maximum values of the velocity can be computed. The variation around the circle at each radius in the far field pattern can be computed.

Program RETURN that computes a single point the far field at a specified value of the velocity aberration can compute the cross section and range correction as the satellite spins in a way that closely simulates actual ranging data. The receiver does not measure the whole pattern. It only sees one point in the diffraction pattern. These simulations tend to show significant variations as the incidence angle on the satellite changes. These variations tend to average out over many orientations if the array is properly designed. The important quantity is the average value and any systematic errors.

5. Signal strength Computation

The cross section data given in this report can be used to estimate signal strengths for laser ranging using the range equation

$$N = \frac{E}{h\nu} G'_T A_S G'_S A_R \frac{T^2}{R^4} \eta \qquad (5.1)$$

Where

N = number of photoelectrons
E = transmitted energy of a single pulse
h = Planck's constant
ν = frequency of the laser light
G'_T = "gain" of the transmitter
A_S = active reflecting area of the satellite array
G'_S = "gain" of the satellite array
A_R = area of the receiving telescope
T = atmospheric transmission factor
η = constant, which may include the quantum efficiency of the receiver,

optical losses in the receiver, etc.

If the transmitted beam is a uniform spot of solid angle Ω_T, the "gain" of the transmitter is given by

$$G'_T = \frac{1}{\Omega_T} \tag{5.2}$$

Similarly the "gain" of the satellite array if the reflected beam is a uniform spot of solid angle Ω_S is

$$G'_S = \frac{1}{\Omega_S} \tag{5.3}$$

This is not the standard definition of gain. In the standard definition a source that radiates equally in all direction has unit gain. The standard definition of the gain is

$$G = \frac{4\pi}{\Omega} \tag{5.4}$$

In other words the standard gain tells us what is the amplification obtained in concentrating the signal in a narrow solid angle Ω rather than having it spread over 4π steradians. The "gain" as defined in equation (5.3) is the amplification obtained in concentrating the signal in a narrow solid angle Ω with respect to the case in which the signal is spread over 1 steradian.

If Ω = 4π the gain is unity. The "gain" defined in equation (5.1) is related to the standard definition of gain by the equation

$$G = 4\pi G'$$

The cross section C is defined as the area times the gain

$$C = AG \tag{5.5}$$

As a function of the "gain", G', the cross section is

$$C = 4\pi AG' \tag{5.6}$$

or

θ ϕ

$$AG' = \frac{C}{4\pi} \tag{5.7}$$

We can define

$$A_S G'_S = \frac{C_S}{4\pi} \tag{5.8}$$

and

$$A_R G'_T = \frac{C_R}{4\pi} \tag{5.9}$$

Substituting equations (5.2) and (5.3) into equation (5.1) gives

$$N = \frac{1}{(4\pi)^2} \frac{E}{h\nu} C_S C_R \frac{T^2}{R^4} \eta \tag{5.10}$$

where C_S and C_R defined by equations (5.8) and (5.9) are the cross sections of the satellite and receiver in standard units. C_S is the cross section of the array being computed in the following sections.

6. Optical cube corner reflectivity.

Reference frames

CCR:
On a single cube corner θ is the azimuth of the incident beam as shown in the figure below and ϕ is measured from the normal to the front face,

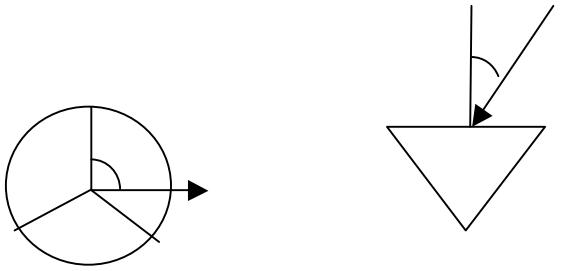

Fig. View of CCR from above the front face (left) from side (right)

Satellite:
On the satellite θ' is the East Longitude and ϕ' is the colatitude (measured from the N pole).

Uncoated cubes can suffer loss of total internal reflection when the incidence angle ϕ is greater than about 17 degrees at θ = -30 deg. There can be total internal reflection out to the absolute cutoff angle of about ϕ = 57 degrees θ = -90 deg. Figure 6.1 below shows the incidence angles where total internal reflection occurs.

The figure is a plot of a 121 x 121 cross section matrix with coordinates (x,y) which go from -60 to +60 deg in each dimension. Each point in the matrix represents an incidence angle (θ,ϕ) where

$$\theta = \tan^{-1}\left(y/x\right) \tag{6.1}$$

and

$$\phi = \sqrt{x^2 + y^2} \tag{6.2}$$

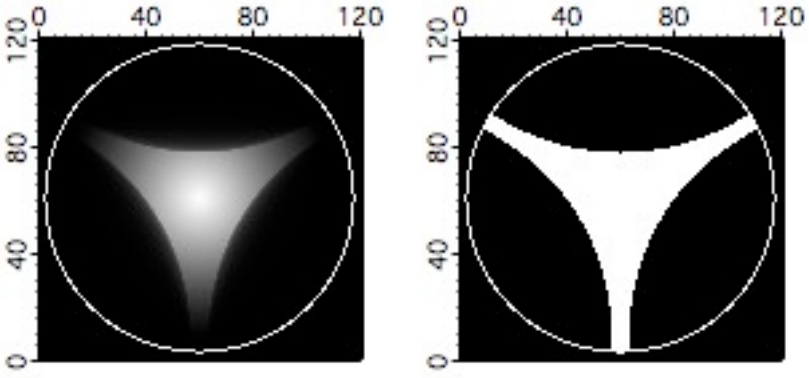

(a) (b)

Figure 6.1. Loss of total internal reflection in an uncoated cube. Part (a) is the total reflected energy vs incidence angle. Part (b) is the region where total internal reflection occurs. The circle is the absolute cutoff angle of the cube corner. There are real back edges pointing up at θ = 90 and at θ = -30 and θ = -150 deg.

The figure below plots the average cross section in the 30 to 45 microradian annulus of the far field diffraction pattern vs incidence angle ϕ for various values of θ.

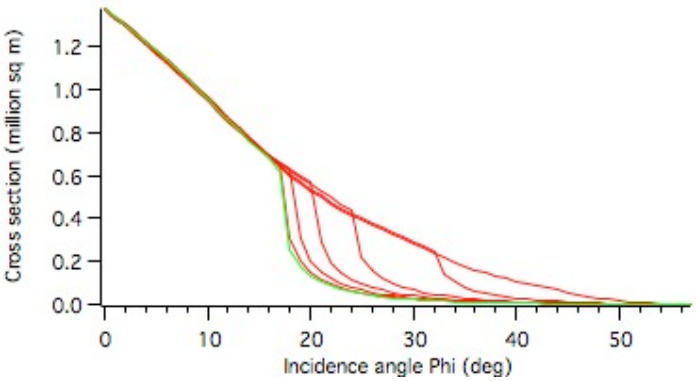

Figure 6.2. Cross section vs incidence angle ϕ for θ = -90,-80,-70,-60,-50,-40, & -30 deg. The top curve is θ = -90 which always has total internal reflection. The successive curves lose total internal reflection earlier. The green curve is for θ = -30 which loses total internal reflection the earliest.

	θ						
ϕ	-90	-80	-70	-60	-50	-40	-30
0.0	1.37286	1.37418	1.37250	1.37290	1.37623	1.37313	1.37454
1.0	1.33538	1.33526	1.33438	1.33310	1.33954	1.33559	1.33712
2.0	1.29727	1.29610	1.29596	1.29370	1.30330	1.29826	1.29889
3.0	1.25845	1.25645	1.25323	1.25263	1.26668	1.25881	1.26106
4.0	1.21893	1.21573	1.21256	1.21204	1.22061	1.22015	1.22203
5.0	1.17583	1.17396	1.17001	1.16712	1.17984	1.18000	1.18160
6.0	1.13634	1.13765	1.12794	1.12519	1.13689	1.13805	1.13933
7.0	1.09536	1.09574	1.08628	1.08046	1.09262	1.09464	1.09583
8.0	1.05288	1.05102	1.04430	1.03645	1.04661	1.04847	1.05013
9.0	1.00910	1.00662	0.99991	0.99083	1.00106	1.00207	1.00338
10.0	0.96347	0.95695	0.95528	0.94360	0.95498	0.95527	0.95541
11.0	0.91853	0.91251	0.91066	0.89811	0.90854	0.90800	0.90704
12.0	0.87219	0.86711	0.86499	0.85275	0.86341	0.86093	0.85871
13.0	0.82496	0.82226	0.82308	0.81020	0.81963	0.81421	0.81125
14.0	0.77627	0.77707	0.77902	0.76888	0.77169	0.77054	0.76542
15.0	0.73064	0.72726	0.73600	0.73160	0.73143	0.72844	0.72175
16.0	0.68503	0.68549	0.69549	0.69448	0.69363	0.68888	0.68080
17.0	0.64190	0.64630	0.65678	0.66060	0.65828	0.65285	0.61316
18.0	0.59970	0.60855	0.62011	0.62844	0.62706	0.30611	0.25679
19.0	0.56292	0.57213	0.58638	0.59731	0.30732	0.20108	0.17587
20.0	0.52878	0.53893	0.55779	0.57153	0.20414	0.14854	0.13188
21.0	0.49712	0.50421	0.52621	0.29223	0.15202	0.11595	0.10360
22.0	0.46791	0.47459	0.49620	0.19700	0.11921	0.09358	0.08383
23.0	0.43828	0.44827	0.46741	0.14833	0.09641	0.07700	0.06915
24.0	0.41537	0.42495	0.44117	0.11712	0.07983	0.06424	0.05780
25.0	0.39346	0.40268	0.21736	0.09513	0.06665	0.05414	0.04873
26.0	0.37133	0.37991	0.15711	0.07921	0.05595	0.04591	0.04130
27.0	0.34882	0.35686	0.12191	0.06609	0.04749	0.03911	0.03512
28.0	0.32257	0.33474	0.09838	0.05571	0.04045	0.03337	0.02996
29.0	0.30305	0.31333	0.08093	0.04717	0.03463	0.02854	0.02565
30.0	0.28288	0.29164	0.06730	0.04013	0.02964	0.02449	0.02197
31.0	0.26170	0.26857	0.05652	0.03447	0.02541	0.02115	0.01887
32.0	0.23953	0.24884	0.04749	0.02931	0.02185	0.01824	0.01628
33.0	0.21566	0.14278	0.04006	0.02518	0.01896	0.01579	0.01421
34.0	0.19459	0.10398	0.03407	0.02150	0.01637	0.01374	0.01234
35.0	0.17680	0.08022	0.02888	0.01843	0.01420	0.01212	0.01079
36.0	0.16168	0.06413	0.02463	0.01605	0.01244	0.01060	0.00954
37.0	0.14771	0.05217	0.02104	0.01372	0.01084	0.00933	0.00852
38.0	0.13399	0.04299	0.01797	0.01187	0.00951	0.00830	0.00750
39.0	0.12074	0.03573	0.01538	0.01028	0.00830	0.00727	0.00665
40.0	0.10869	0.03001	0.01310	0.00885	0.00722	0.00638	0.00586
41.0	0.09756	0.02526	0.01120	0.00764	0.00627	0.00557	0.00510
42.0	0.08681	0.02133	0.00943	0.00650	0.00532	0.00478	0.00444
43.0	0.07643	0.01756	0.00791	0.00549	0.00453	0.00408	0.00381
44.0	0.06643	0.01455	0.00660	0.00460	0.00381	0.00342	0.00323
45.0	0.05649	0.01189	0.00542	0.00377	0.00316	0.00283	0.00264
46.0	0.04697	0.00940	0.00429	0.00300	0.00250	0.00224	0.00211
47.0	0.03810	0.00726	0.00333	0.00233	0.00194	0.00175	0.00166
48.0	0.02986	0.00550	0.00251	0.00175	0.00146	0.00131	0.00123
49.0	0.02260	0.00390	0.00178	0.00124	0.00103	0.00093	0.00088

50.0	0.01645	0.00270	0.00123	0.00085	0.00071	0.00064	0.00061
51.0	0.01136	0.00179	0.00081	0.00056	0.00046	0.00042	0.00040
52.0	0.00738	0.00112	0.00050	0.00035	0.00029	0.00026	0.00024
53.0	0.00443	0.00065	0.00029	0.00020	0.00016	0.00015	0.00014
54.0	0.00231	0.00033	0.00015	0.00010	0.00008	0.00007	0.00007
55.0	0.00096	0.00014	0.00006	0.00004	0.00003	0.00003	0.00003
56.0	0.00025	0.00003	0.00002	0.00001	0.00001	0.00001	0.00001

Table 6.2. Data used to plot Fig 6.2. Cross section of a single LARES cube in the 30 to 45 microradian annulus of the far field diffraction pattern vs ϕ for various values of θ. The incident beam has circular polarization.

The diffraction pattern of an uncoated cube corner is complicated particularly when dihedral angle offsets are included. The figures below show how the pattern of a LARES cube changes with incidence angle ϕ at θ = -90 and -30 deg. At -90 deg there is no loss of total internal reflection. At -30 there is loss of total internal reflection past ϕ = 17 deg. The incident beam has circular polarization. However, this does not produce a perfectly symmetrical pattern. The pattern becomes very unsymmetrical particularly for θ = -30 deg where there is loss of total internal reflection. After loss of total internal reflection there is still ordinary reflection (i.e. part of the energy is lost by transmission) at one back face and total internal reflection at the other two faces. At ϕ = 0, θ is indeterminate. The orientation of the patterns has been choses so that it is the same as if there were a very small value of ϕ.

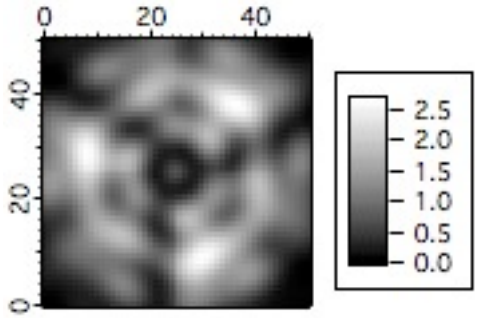

θ = -90, ϕ = 0

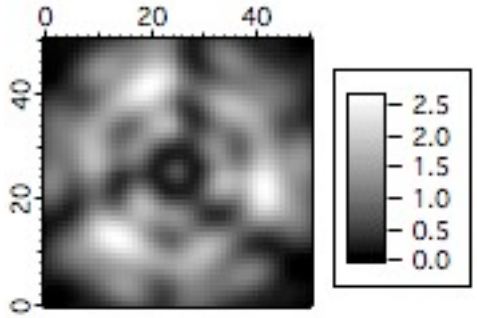

θ = -30, ϕ = 0

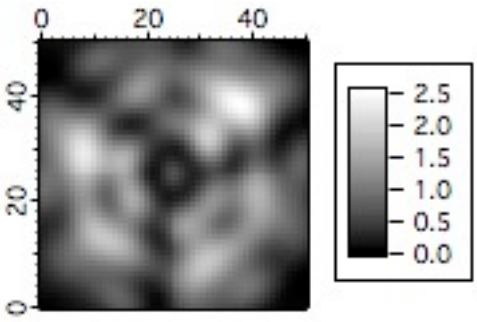

θ = -90, ϕ = 5

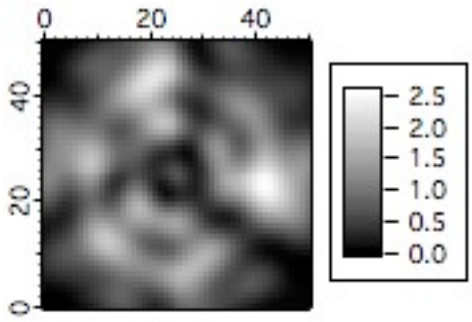

θ = -30, ϕ = 5

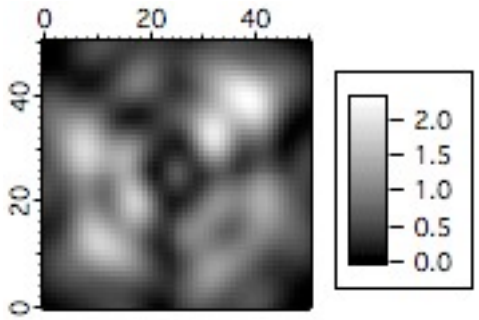

θ = -90, ϕ = 10

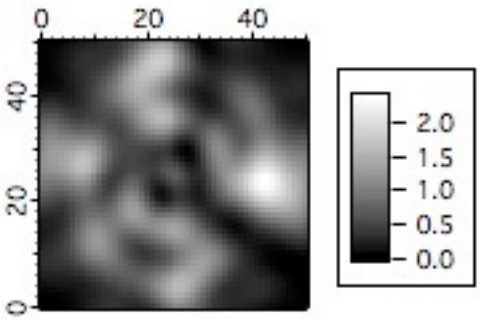

θ = -30, ϕ = 10

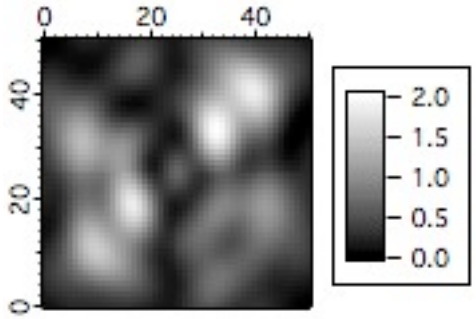

θ = -90, ϕ = 15

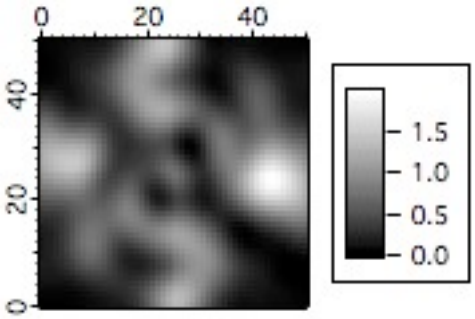

θ = -30, ϕ = 15

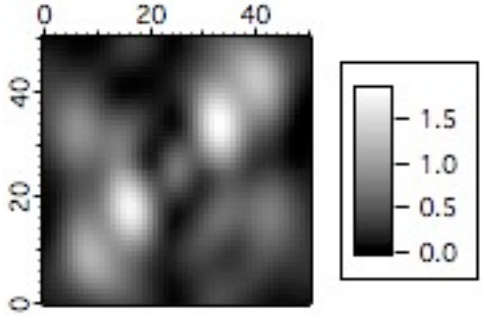

θ = -90, ϕ = 20

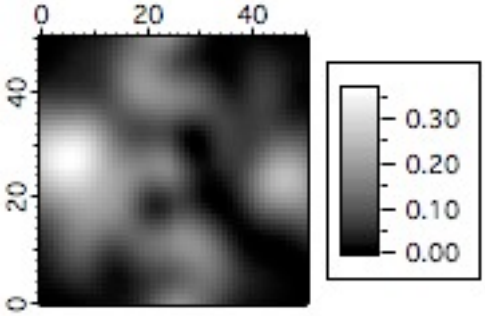

θ = -30, ϕ = 20

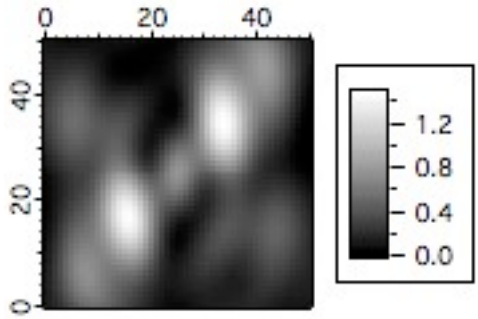

θ = -90, ϕ = 25

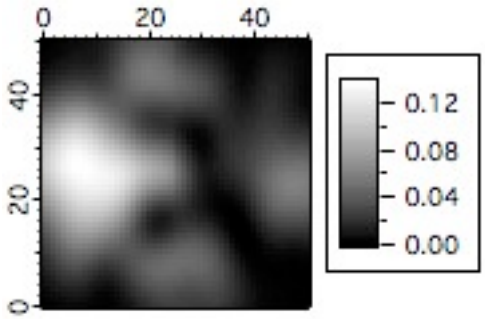

θ = -30, ϕ = 25

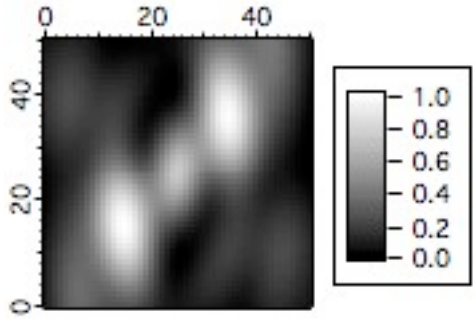

θ = -90, ϕ = 30

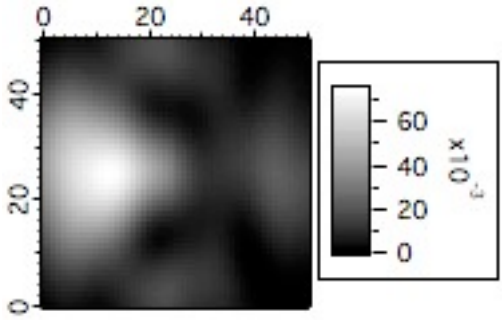

θ = -30, ϕ = 30

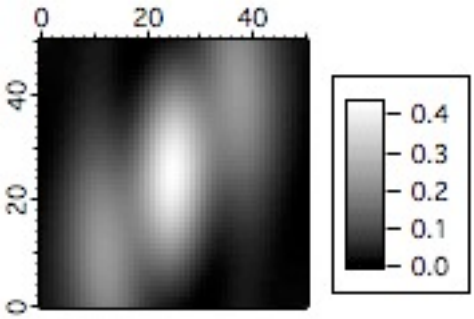

θ = -90, ϕ = 40

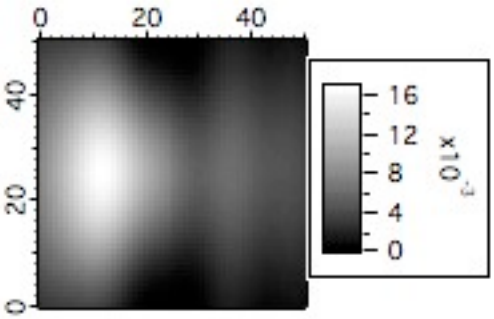

θ = -30, ϕ = 40

7. Variation of the transfer function with incidence angle on the satellite.

The cross section and range correction are a function of the incidence angle on the satellite and the velocity aberration. The incidence angle can be described by two angles. The velocity aberration has two components which can be specified in any convenient coordinate system such as the horizontal and vertical components with respect to the local horizon. At each incidence angle the distribution of reflectors along the line of sight will be different. With uncoated cubes the transfer function also depends on the

polarization of the transmitted beam. For linear polarization there is a dependence on the direction of the polarization. The surface of LARES is covered with cube corners as uniformly as possible to minimize systematic effects with the incidence angle. Although there can be significant variations with incidence angle and velocity aberration these differences should average out over a large number of observations. Since the satellite is unstabilized and the attitude is unknown there is no way to calculate range corrections for each observation.

In order to determine the average transfer function simulations have been done over many incidence angles using program TRANSFR (described in section 4) which compute the centroid range matrix and the cross section matrix. An incidence angle that has close to the average range correction and cross section is then selected for detailed studies using program RETURN that can compute more complicated properties of the return signal. The simulation program has the ability to start from a particular incidence angle and then increment each angle by a specified amount in order to perform a large number of simulations within a single computer run. The incidence angles are specified by the longitude θ' and colatitude ϕ' on the satellite. In order to cover a large part of the satellite in a single run the longitude is started at 0 deg and incremented by 5 deg between each simulation. The colatitude is started at 15 degrees and incremented by .07 degree between each simulation. After 1080 simulations the colatitude has changed by 75.6 degrees which brings it just past the equator. The longitude changes by one revolution after 72 simulations. In that time the colatitude changes by about 5 degrees. The incidence angle spirals down the satellite. Since the rows of cube corners are every 20 degrees there are 4 revolutions around the satellite between each ring of cube corners. Hopefully this simulation going from $\phi = 15$ deg to just beyond the equator at $\phi = 90$ deg gives a reasonably good selection of orientations to determine the average behavior.

8. Reflectivity histogram.

Simulations have been done for the set of 1080 incidence angles described in the last section. At each incidence angle the average cross section of each active cube corner is computed in the velocity aberration annulus between 30 and 45 microradians. The cross section and position of each cube corner along the line of sight is tabulated for each orientation. The contributions from all the cube corners at all the incidence angles is summed in 2 mm bins in order to create an average histogram of the return signal. This data is than normalized to a peak value of unity. The result is shown the in figure below.

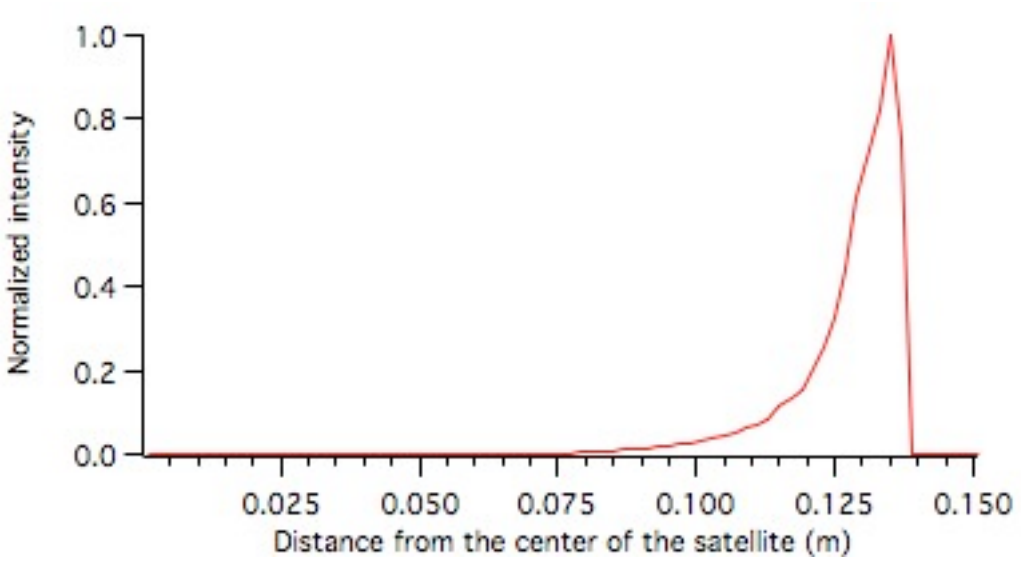

Figure 8.1. Histogram of the return pulse from LARES (2 mm bins).

The curve has a break in slope at around 130 mm. This is due to loss of total internal reflection for large incidence angles on the cube corner. Loss of total internal reflection has the effect of reducing the return pulse width by reducing the contribution of cube corners that are at large incidence angles. Since the array is spherical, large incidence angles are further from the point of closest approach.

The table below gives the data used to plot figure 8.1

Distance	Signal
0.051000	0.000000
0.053000	0.000000
0.055000	0.000000
0.057000	0.000000
0.059000	0.000001
0.061000	0.000014
0.063000	0.000051
0.065000	0.000159
0.067000	0.000373
0.069000	0.000575
0.071000	0.000773
0.073000	0.001485
0.075000	0.001663
0.077000	0.002764
0.079000	0.004137
0.081000	0.004995
0.083000	0.006369
0.085000	0.007699
0.087000	0.009970
0.089000	0.013910
0.091000	0.014834
0.093000	0.017862
0.095000	0.021286

0.097000	0.023188
0.099000	0.028373
0.101000	0.031733
0.103000	0.039818
0.105000	0.043994
0.107000	0.051461
0.109000	0.062436
0.111000	0.072866
0.113000	0.085397
0.115000	0.111904
0.117000	0.133055
0.119000	0.153726
0.121000	0.206601
0.123000	0.254958
0.125000	0.322945
0.127000	0.439868
0.129000	0.612228
0.131000	0.728307
0.133000	0.823681
0.135000	1.000000
0.137000	0.754570
0.139000	0.000000
0.141000	0.000000
0.143000	0.000000
0.145000	0.000000
0.147000	0.000000
0.149000	0.000000
0.151000	0.000000

Table 8.1. Histogram data used to plot figure 8.1

9. Array reflectivity

The cross section matrix is different at every incidence angle on the satellite. In order to compute the average cross section matrix simulations have been done for the 1080 incidence angles described at the end of section 7. The figure below shows the average cross section matrix for circular and linear vertical polarization with the nominal dihedral angle offset of 1.5 arcseconds. This is a 51 x 51 matrix from -50 to 50 microradians in each direction.

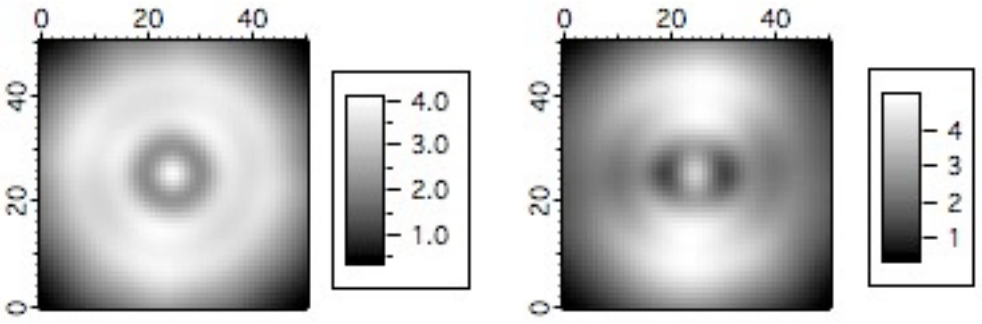

(a) (b)

Figure 9.1. Average cross section matrix (million sq m) over 1080 incidence angles for circular polarization (a) and linear vertical polarization (b). The cross section matrix has circular symmetry for circular polarization. However, it is asymmetric for linear vertical polarization.

The tables below show the variation of the cross section vs velocity aberration within the diffraction pattern. These tables have been computed by averaging the cross section around circles of increasing radius in the far field pattern. The radius is varied from 0 to 50 microradians in 2 microradian increments. The minimum, average, maximum and maximum – minimum around the circles are computed for each radius.

The table below is for circular polarization.

Microrad	Minimum	Average	Maximum	Max - Min
0.0	3.9780120	3.9780120	3.9780120	0.0000000
2.0	3.7579022	3.7812858	3.8250690	0.0671668
4.0	3.3539188	3.3786570	3.4226360	0.0687172
6.0	2.8283753	2.8726171	2.9172529	0.0888776
8.0	2.3736078	2.4366972	2.4903035	0.1166957
10.0	2.1318200	2.2095615	2.2683600	0.1365401
12.0	2.1609780	2.2464740	2.3222420	0.1612640
14.0	2.4188568	2.5091025	2.6204242	0.2015674
16.0	2.7741705	2.8889825	3.0449483	0.2707778
18.0	3.1106163	3.2569379	3.4548219	0.3442056
20.0	3.3416437	3.5163660	3.7491465	0.4075029
22.0	3.4312308	3.6309237	3.8900149	0.4587841
24.0	3.4043578	3.6252645	3.9005924	0.4962347
26.0	3.3232247	3.5614515	3.8452851	0.5220604
28.0	3.2495055	3.5023879	3.7872875	0.5377820
30.0	3.2203846	3.4838603	3.7639918	0.5436072
32.0	3.2355320	3.5019471	3.7812183	0.5456862
34.0	3.2542555	3.5267275	3.8070036	0.5527481
36.0	3.2423361	3.5160443	3.8070693	0.5647333
38.0	3.1740589	3.4430236	3.7444565	0.5703977
40.0	3.0374560	3.3021449	3.6094485	0.5719925
42.0	2.8439472	3.1067139	3.4146347	0.5706875
44.0	2.6256420	2.8808232	3.1837354	0.5580934
46.0	2.3983795	2.6473437	2.9389379	0.5405584
48.0	2.1756966	2.4180238	2.6908475	0.5151508
50.0	1.9616194	2.1938772	2.4442289	0.4826094

Table 9.1. Average cross section (million sq m) over 1080 incidence angles vs velocity aberration (microradians) for circular polarization, dihedral angle 1.5 arcseconds.

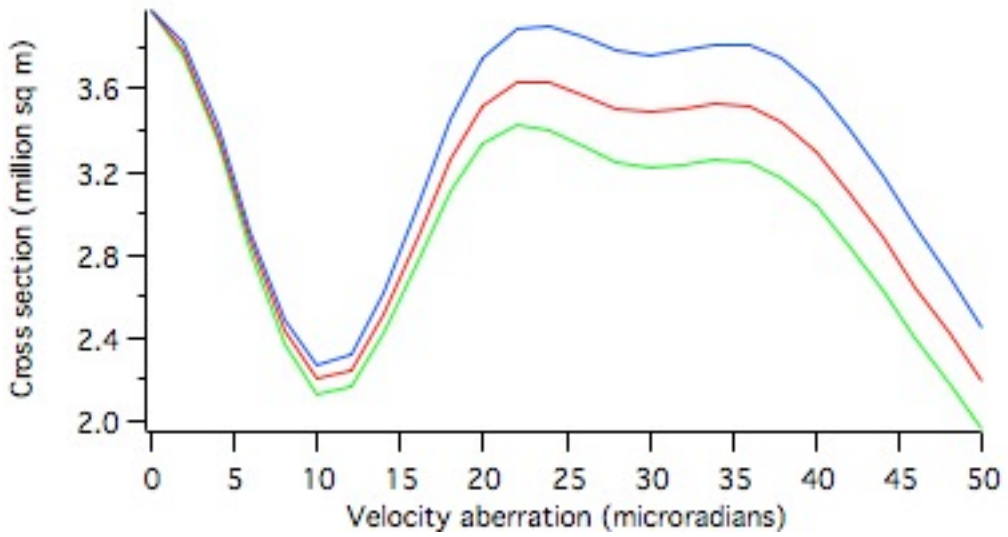

Figure 9.2. Average cross section over 1080 incidence angles vs velocity aberration with circular polarization, dihedral angle offset 1.5 arcseconds.
Green = minimum
Red = average
Blue = maximum

The table below is for linear vertical polarization.

Microrad	Minimum	Average	Maximum	Max - Min
0.0	4.0000730	4.0000730	4.0000730	0.0000000
2.0	3.7639994	3.8027729	3.8882880	0.1242886
4.0	3.2296474	3.3987608	3.5991370	0.3694896
6.0	2.5284088	2.8903905	3.2552230	0.7268142
8.0	1.8769150	2.4512493	3.0030430	1.1261280
10.0	1.4510090	2.2201997	2.9531770	1.5021680
12.0	1.3347820	2.2529305	3.1400940	1.8053120
14.0	1.4842680	2.5116229	3.5138510	2.0295830
16.0	1.7951270	2.8883923	3.9740134	2.1788864
18.0	2.1208090	3.2544649	4.3933790	2.2725700
20.0	2.3442420	3.5133480	4.6888457	2.3446037
22.0	2.4160980	3.6285456	4.8423022	2.4262042
24.0	2.3589140	3.6241095	4.8806638	2.5217498
26.0	2.2411190	3.5618556	4.8599036	2.6187846
28.0	2.1372550	3.5037405	4.8374227	2.7001677
30.0	2.0940660	3.4855178	4.8397517	2.7456857
32.0	2.1161240	3.5032111	4.8569574	2.7408334
34.0	2.1734030	3.5271406	4.8538199	2.6804169
36.0	2.2211174	3.5152273	4.7948969	2.5737795
38.0	2.2196585	3.4412607	4.6487178	2.4290592
40.0	2.1659224	3.2998908	4.4138678	2.2479454
42.0	2.0714047	3.1044223	4.1104848	2.0390801
44.0	1.9581072	2.8788705	3.7683235	1.8102163
46.0	1.8452354	2.6459668	3.4139291	1.5686937
48.0	1.7409979	2.4173121	3.0612861	1.3202882

50.0	1.6378156	2.1937098	2.7181174	1.0803018

Table 9.2 Average cross section (million sq m) over 1080 incidence angles vs velocity aberration (microradians) for linear vertical polarization. The maximum cross section is higher than for circular polarization and the differences around the circle are greater.

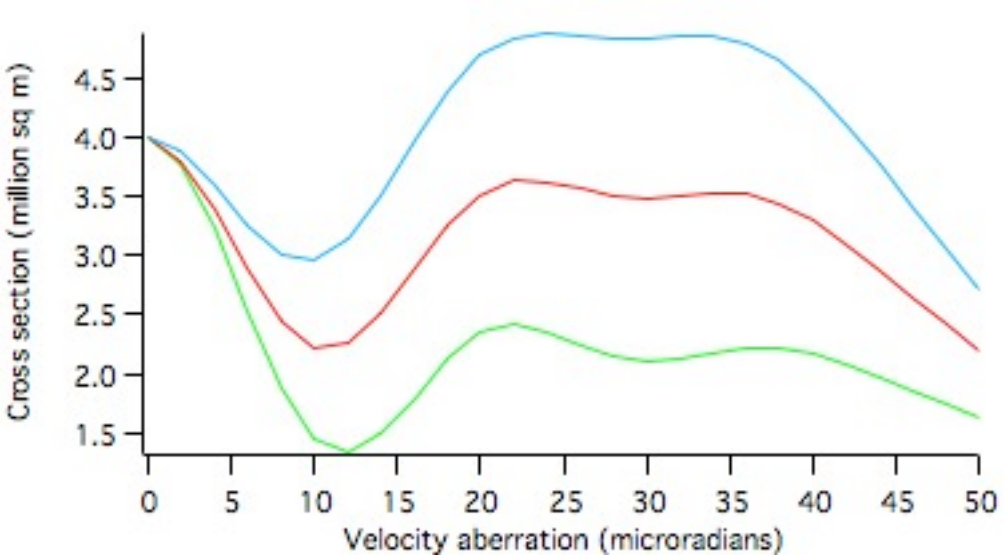

Figure 9.3. Average cross section over 1080 incidence angles vs velocity aberration with linear vertical polarization, dihedral angle offset 1.5 arcseconds.
Green = minimum
Red = average
Blue = maximum

The data presented previously in this section is the average over many incidence angles and over the whole far field pattern. The receiver only sees one point the far field pattern. The graph below shows how the cross section varies at a single point in the far field pattern as the incidence angles spirals from colatitude 15 deg to the equator at colatitude 90 deg.

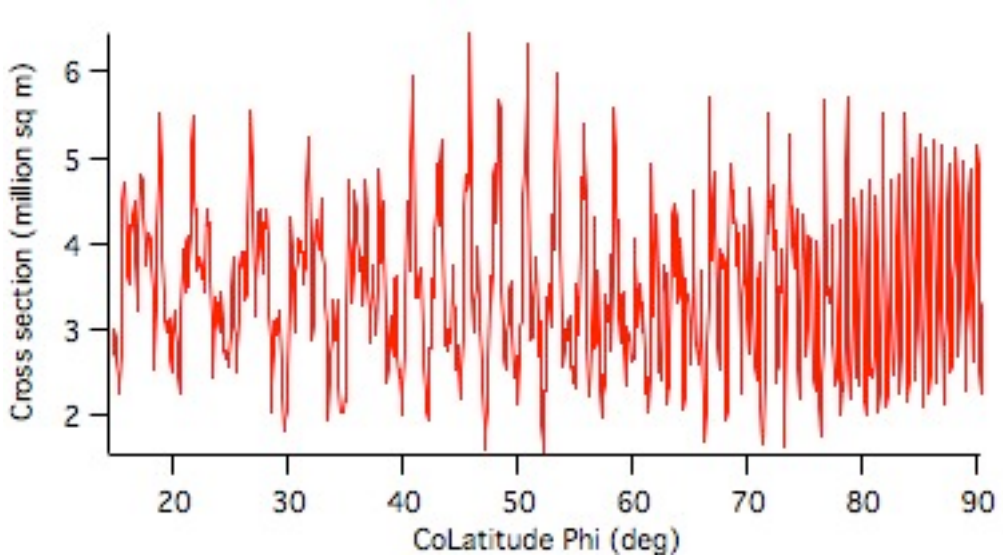

Figure 9.4. Cross section at velocity aberration (36,0) microradians where 36 in the horizontal position and 0 is the vertical position. The Longitude starts at 0 and increments 5 deg between points. The colatitude starts at 15 deg and increments at .07 deg between points. The colatitude increases by 5 deg as the Longitude goes from 0 to 360 deg. Since the arcdistance between points is smaller at 15 deg colatitude and larger at 90 deg colatitude (the equator) the frequency of the variations increases toward the equator. The rows of cube corners are at colatitude 20,40,60,and 80 degrees. There does not seem to be any systematic effect as the incidence angle goes across each row of cubes. The dihedral angle offset is 1.5 arcsec and the polarization is circular.

10. Range correction.

Contents of section 10.

The primary range correction computed by the analysis programs is the centroid of the return signal. The half maximum point on the leading edge can also be computed. This requires plotting the pulse shape and depends on pulse length. The program that does this computes only a single point in the far field. Since LARES is an unstabilized spherical satellite the quantity of interest is the average range correction over many orientations. The range correction matrix at a single orientation is irregular. However, the average range correction over many orientations takes a regular shape that depends on the polarization.

10.1 Average range correction matrix over many incidence angles.

The plots below show the effect of averaging a large number of range correction matrices at different incidence angles. Simulations have been done for both circular and linear vertical polarization. For these cases the longitude has been started at 0 deg and the colatitude at 90 deg (equatorial). The longitude is incremented by 5 deg between points and the colatitude by .07 deg. The first set of plots is for circular polarization. The number below is the number of points averaged.

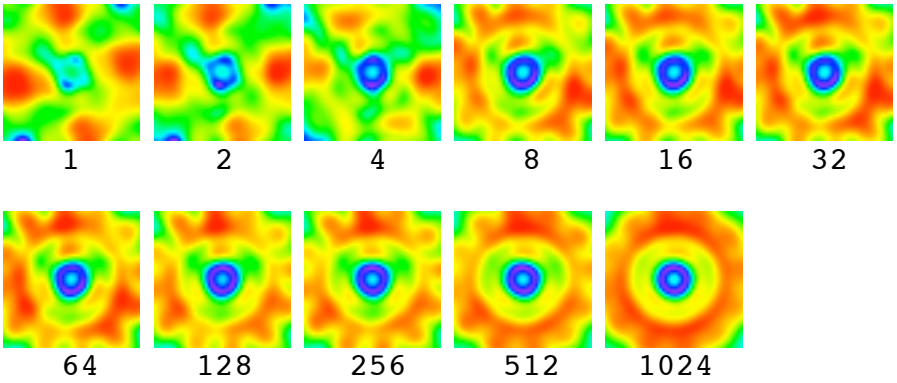

Figure 10.1. Figures 1 through 1024 show the effect of averaging increasing numbers of matrices. By the time 1024 matrices have been averaged the plot has become reasonably circular. The dihedral angle is 1.5 arcsec and the polarization is circular.

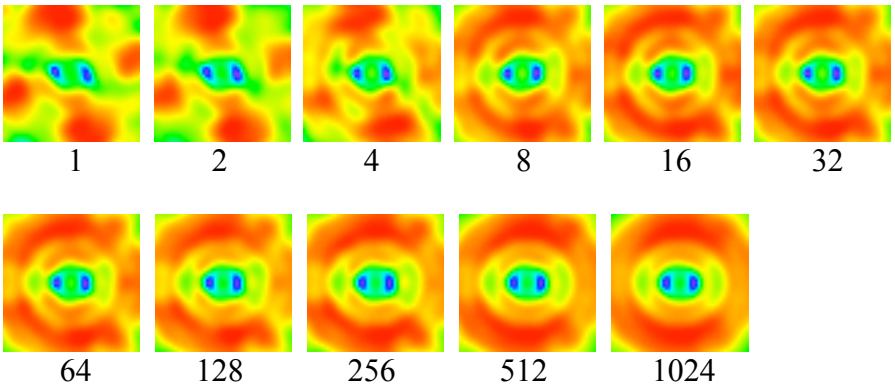

Figure 10.2. Figures 1 through 1024 show the effect of averaging increasing numbers of matrices. Averaging 1024 matrices produces a fairly regular pattern that has symmetry from right to left. The dihedral angle is 1.5 arcsec and linear vertical polarization is used.

The next two plots have been done using 1080 incidence angles between colatitude 15 and 90 deg with the Longitude incrementing 5 deg between points and the colatitude incremented .07 deg between points. This causes the incidence angle to spiral down to the equator.

The figures below shows the average centroid range correction over 1080 incidence angles with circular and linear polarization. The matrix is 51 x 51 pixels from -50 to +50 microradians in each axis with 2 microradians between pixels.

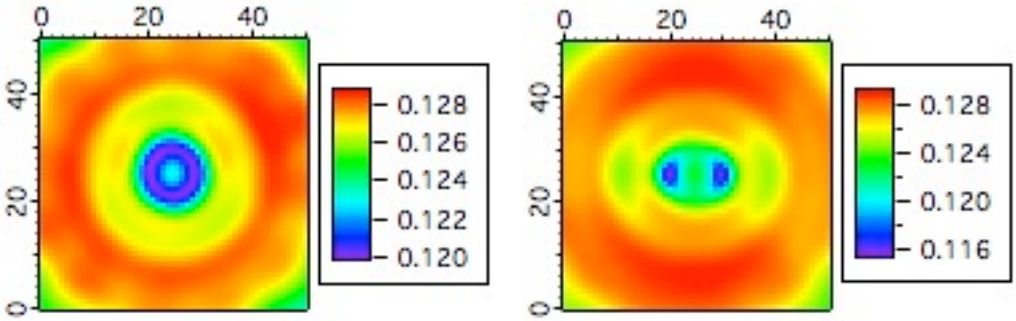

(a) (b)

Figure 10.3. Average centroid range correction (m) over 1080 incidence angles for circular polarization (a) and linear vertical polarization (b). For circular polarization the pattern has nearly circular symmetry. For linear vertical polarization the pattern is asymmetric. There is a systematic variation of the range correction around a circle in the far field pattern with linear polarization.

The figure below show the average centroid around circles of increasing radius in the far field. The radius is incremented by 2 microadians between circles. For each circle the minimum, average, and maximum values are computed.

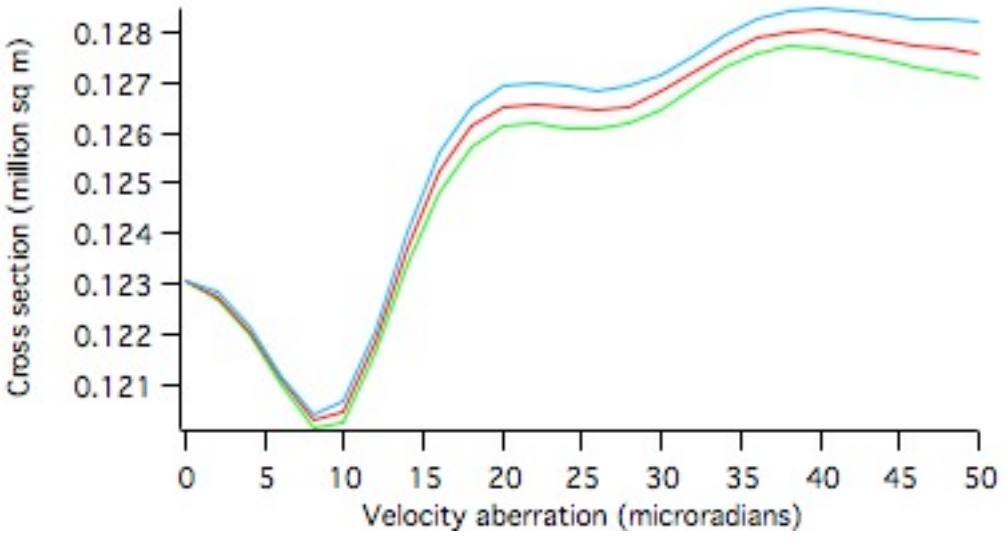

Figure 10.4. Centroid range correction shown in figure 10.3.a averaged over circles of increasing radius in the far field vs velocity aberration with circular polarization and dihedral angle offset 1.5 arcseconds. The region of interest is 30 to 45 microradians. The range correction is lowest at 30 microradians.

Green = minimum around the circle

Red = average around the circle
Blue = maximum around the circle

The table below shows the data used to plot figure 10.4.

Microrad	Minimum	Average	Maximum	Max - Min
0.0	0.1230400	0.1230400	0.1230400	0.0000000
2.0	0.1227027	0.1227402	0.1228100	0.0001073
4.0	0.1220052	0.1220513	0.1221300	0.0001248
6.0	0.1209977	0.1210667	0.1211400	0.0001423
8.0	0.1201224	0.1202653	0.1204010	0.0002786
10.0	0.1202200	0.1204287	0.1206411	0.0004211
12.0	0.1215919	0.1218150	0.1220414	0.0004495
14.0	0.1233623	0.1236912	0.1239945	0.0006323
16.0	0.1248280	0.1252115	0.1255974	0.0007694
18.0	0.1257251	0.1261152	0.1265140	0.0007889
20.0	0.1261176	0.1265050	0.1269331	0.0008156
22.0	0.1261688	0.1265671	0.1270022	0.0008335
24.0	0.1260850	0.1264914	0.1269088	0.0008238
26.0	0.1260600	0.1264449	0.1268437	0.0007837
28.0	0.1261800	0.1265348	0.1269183	0.0007383
30.0	0.1264800	0.1268024	0.1271719	0.0006919
32.0	0.1268800	0.1271820	0.1275440	0.0006640
34.0	0.1272800	0.1275729	0.1279446	0.0006646
36.0	0.1275776	0.1278680	0.1282598	0.0006822
38.0	0.1277081	0.1280209	0.1284360	0.0007278
40.0	0.1276945	0.1280374	0.1284773	0.0007828
42.0	0.1275844	0.1279595	0.1284327	0.0008483
44.0	0.1274450	0.1278456	0.1283464	0.0009015
46.0	0.1273204	0.1277395	0.1282783	0.0009579
48.0	0.1272155	0.1276556	0.1282439	0.0010284
50.0	0.1271107	0.1275786	0.1282066	0.0010959

Table10.1. Minimum, average, maximum, and max - min range correction (m) for the matrix of figure 10.3.a vs velocity aberration (microradians) for circular polarization, dihedral angle 1.5 arcseconds. The values are around circles in the far field of radius given in the first column. The largest difference in range around a circle in the far field is about .9 mm at 45 microradians.

The figure below shows the range correction of figure 10.3.b with linear polarization vs velocity aberration.

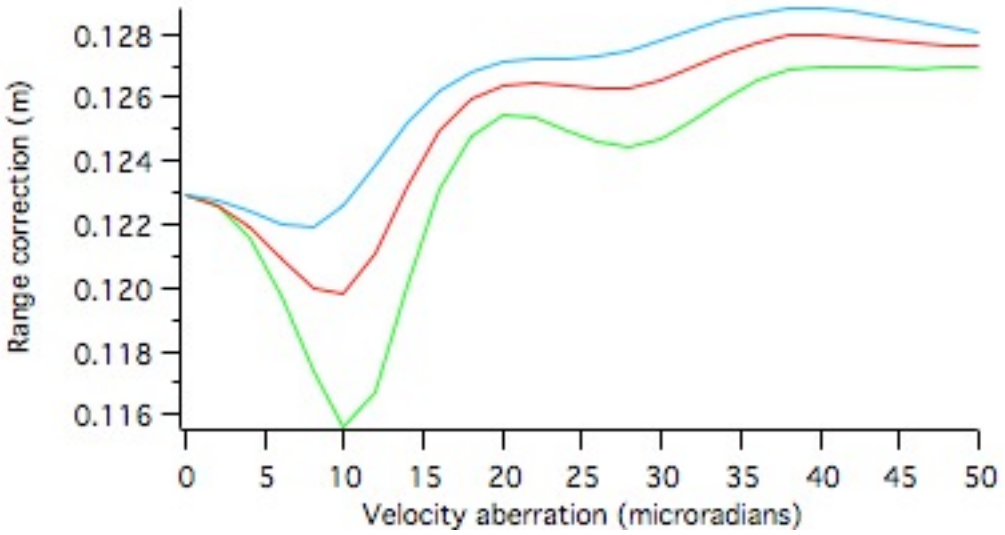

Figure 10.5. Centroid range correction for the matrix shown in figure 10.3.b vs velocity aberration with linear vertical polarization and dihedral angle offset 1.5 arcseconds. The region of interest is 30 to 45 microradians. The range correction is lowest at 30 microradians. The variation in range around a circle in the far field is larger with linear polarization.

Green = minimum around the circle
Red = average around the circle
Blue = maximum around the circle

The table below shows the data used to plot figure 10.5.

Microrad	Minimum	Average	Maximum	Max - Min
0.0	0.1229100	0.1229100	0.1229100	0.0000000
2.0	0.1225518	0.1226189	0.1227700	0.0002182
4.0	0.1215550	0.1219442	0.1224000	0.0008450
6.0	0.1197700	0.1209331	0.1219900	0.0022200
8.0	0.1173500	0.1199702	0.1219400	0.0045900
10.0	0.1156100	0.1198384	0.1225700	0.0069600
12.0	0.1166800	0.1211053	0.1238237	0.0071437
14.0	0.1200300	0.1231581	0.1251735	0.0051435
16.0	0.1230600	0.1249006	0.1262116	0.0031516
18.0	0.1247800	0.1259441	0.1268287	0.0020487
20.0	0.1254100	0.1263941	0.1271158	0.0017058
22.0	0.1253700	0.1264598	0.1272058	0.0018358
24.0	0.1249700	0.1263501	0.1272300	0.0022600
26.0	0.1245700	0.1262537	0.1273100	0.0027400
28.0	0.1244300	0.1263062	0.1274900	0.0030600
30.0	0.1246800	0.1265651	0.1277800	0.0031000
32.0	0.1252500	0.1269676	0.1281200	0.0028700
34.0	0.1259300	0.1273990	0.1284400	0.0025100
36.0	0.1265146	0.1277379	0.1286800	0.0021654
38.0	0.1268720	0.1279284	0.1288100	0.0019380
40.0	0.1269892	0.1279726	0.1288100	0.0018208

42.0	0.1269704	0.1279143	0.1287200	0.0017496
44.0	0.1269185	0.1278150	0.1285700	0.0016515
46.0	0.1269066	0.1277230	0.1284039	0.0014973
48.0	0.1269631	0.1276556	0.1282428	0.0012797
50.0	0.1269477	0.1275950	0.1280652	0.0011174

Table10.2. Centroid range correction (m) for the matrix shown in figure 10.3.b vs velocity aberration (microradians) for linear vertical polarization and dihedral angle 1.5 arcseconds. The values are around circles in the far field of radius given in the first column. The largest difference in range around a circle in the far field is about 3.1 mm at 30 microradians. This is due to the asymmetry in the pattern as seen in figure 10.3.b.

The figure below compares the range correction vs velocity aberration for circular and linear polarization.

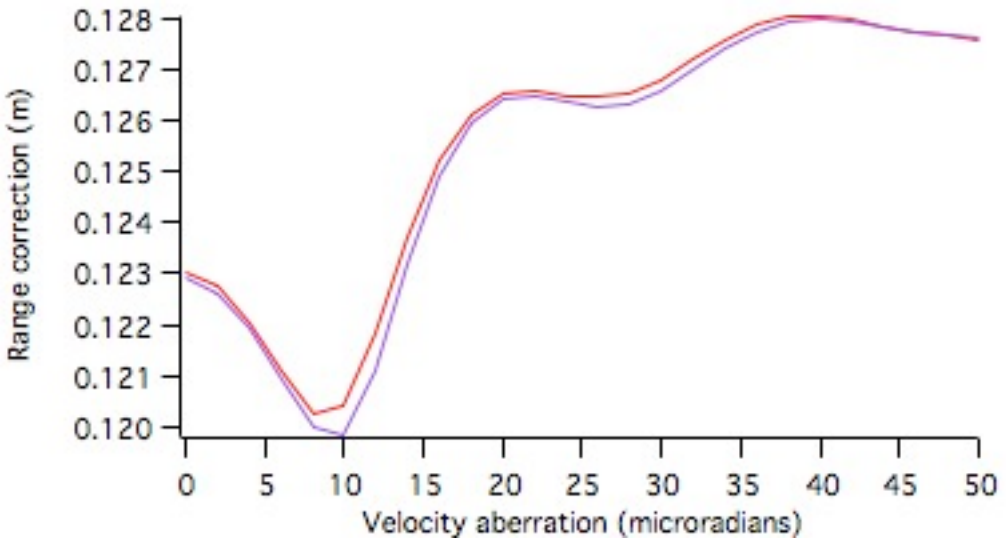

Figure 10.6. Centroid range correction vs velocity aberration with circular polarization (red) and linear vertical polarization (purple) with dihedral angle offset 1.5 arcseconds. There is very little difference in the average around a circle in the far field for the two polarizations. The main difference is that the pattern for linear polarization is asymmetrical. The range correction depends on the angle between the velocity aberration and the polarization vector.

10.2 Dependence of the centroid range correction on dihedral angle offset

The tolerance on the dihedral angle offset of the LARES cube corners is specified as 90° + 1.5” +/- 0.5”. The dihedral angle can vary between 1.00 and 2.00 arcsec with this tolerance. The average range correction matrix has been computed for 1080 incidence angles between 15 and 90 degrees colatitude on the LARES satellite for 5 different dihedral angle offsets, 1.00, 1.25, 1.50, 1.75, and 2.00 arcsec. The range correction is computed vs the magnitude of the velocity aberration by averaging the

range correction around circles in the far field pattern. The results are plotted below.

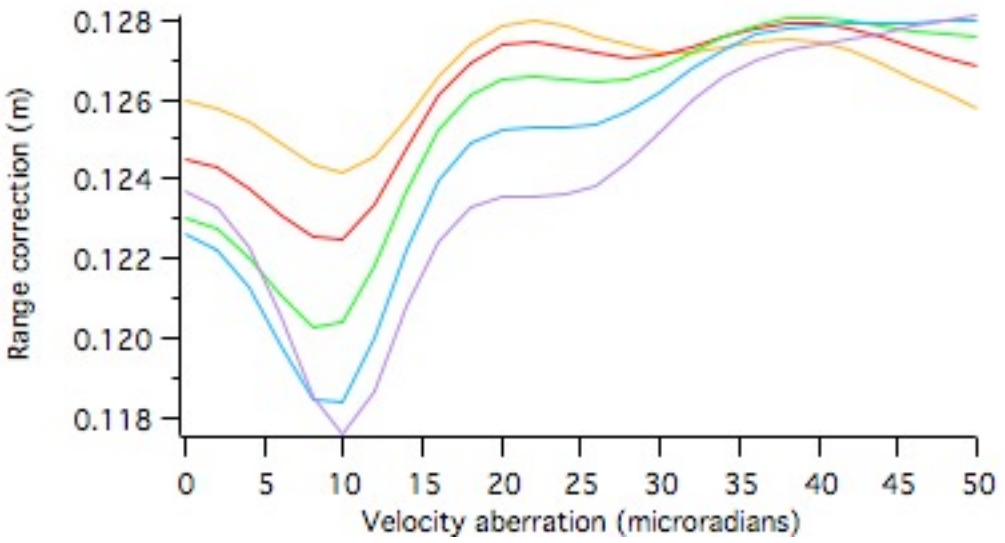

Figure 10.7. Range correction vs velocity aberration for 5 different dihedral angle offsets.

Color	Arcsec	Range correction (m) 30 – 45 microradians
Yellow	1.00	.1273
Red	1.25	.1277
Green	1.50	.1278
Blue	1.75	.1276
Purple	2.00	.1270

If the average dihedral angle offset is 1.50 arcsec the range correction vs velocity aberration is given by the green curve. The average range correction over the 30 – 45 microradian interval changes by less than a millimeter. However the range correction is a function of the magnitude of the velocity aberration. The range correction is increasing with dihedral angle offset up to 1.50 arcsec and then decreases for larger offsets.

The plot below shows the region between 30 and 45 microradians in expanded detail.

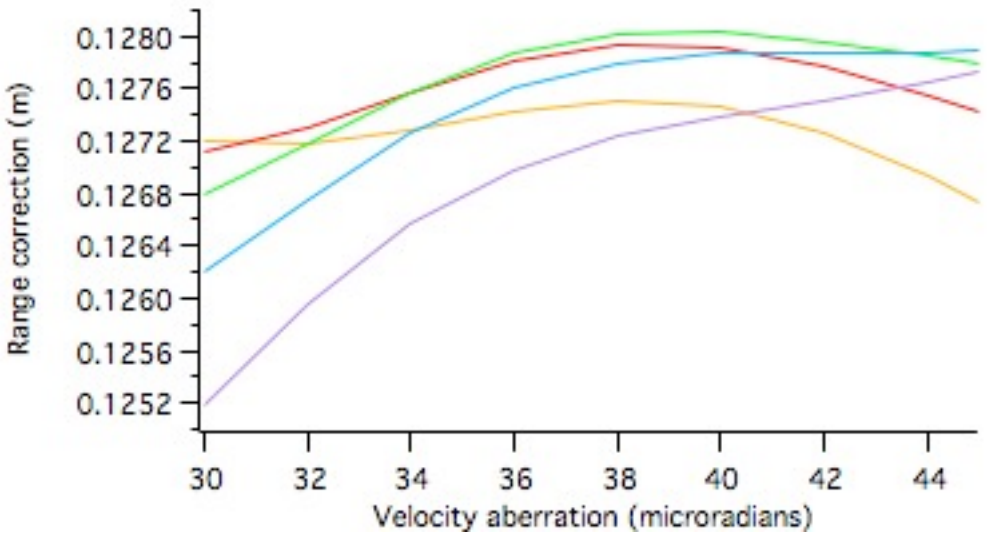

Figure 10.8. Expanded plot for figure 10.7 between 30 and 45 microradians.

Color	Arcsec
Yellow	1.00
Red	1.25
Green	1.50
Blue	1.75
Purple	2.00

10.3. Centroid range correction with the actual dihedral angle offsets.

Section 2 lists the actual dihedral angle offsets. Simulations have been done for 1080 incidence angles using the actual dihedral angle offsets. The figure below shows the range correction vs dihedral angle offset.

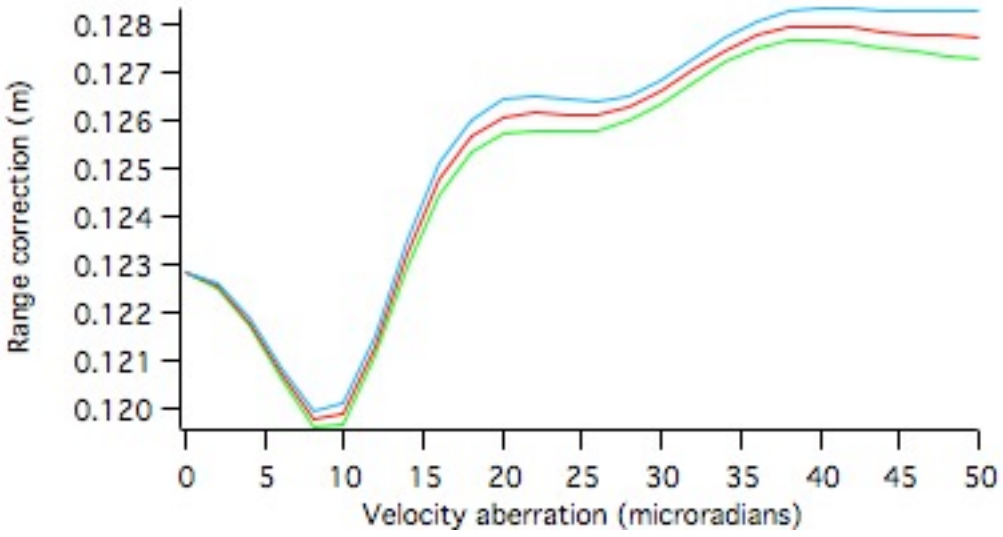

Figure 10.9. Range correction vs velocity aberration averaged over 1080 orientations using the actual dihedral angle offsets for LARES with circular polarization.

The table below shows the data used to plot figure 10.9.

Microrad	Minimum	Average	Maximum	Max - Min
0.0	0.1228600	0.1228600	0.1228600	0.0000000
2.0	0.1224994	0.1225411	0.1226200	0.0001206
4.0	0.1217531	0.1217982	0.1218900	0.0001369
6.0	0.1206327	0.1207133	0.1208200	0.0001873
8.0	0.1196209	0.1197946	0.1199379	0.0003169
10.0	0.1196600	0.1198955	0.1201120	0.0004520
12.0	0.1211193	0.1213041	0.1215260	0.0004067
14.0	0.1229419	0.1232296	0.1235120	0.0005701
16.0	0.1244267	0.1247780	0.1251067	0.0006800
18.0	0.1253251	0.1256876	0.1260199	0.0006948
20.0	0.1257162	0.1260760	0.1264247	0.0007086
22.0	0.1257864	0.1261447	0.1264939	0.0007075
24.0	0.1257506	0.1260938	0.1264225	0.0006719
26.0	0.1257797	0.1260964	0.1263905	0.0006108
28.0	0.1259798	0.1262544	0.1265237	0.0005439
30.0	0.1263479	0.1265930	0.1268511	0.0005032
32.0	0.1267946	0.1270283	0.1272851	0.0004906
34.0	0.1272066	0.1274531	0.1277235	0.0005169
36.0	0.1275126	0.1277645	0.1280582	0.0005457
38.0	0.1276588	0.1279288	0.1282516	0.0005927
40.0	0.1276690	0.1279638	0.1283276	0.0006586
42.0	0.1275943	0.1279181	0.1283175	0.0007232
44.0	0.1274952	0.1278470	0.1282834	0.0007882
46.0	0.1274145	0.1277905	0.1282687	0.0008542
48.0	0.1273563	0.1277551	0.1282709	0.0009147
50.0	0.1272947	0.1277216	0.1282705	0.0009758

Table 10.3. Range correction vs velocity aberration using the actual dihedral angle offsets with circular polarization. This table should be the best estimate of the range correction with circular polarization. The range correction varies by 1.3 millimeters in the range 30 to 45 microradians.

The figure below shows the difference between using 1.50 arcsec and using the actual dihedral angles which average about 1.58 arcsec.

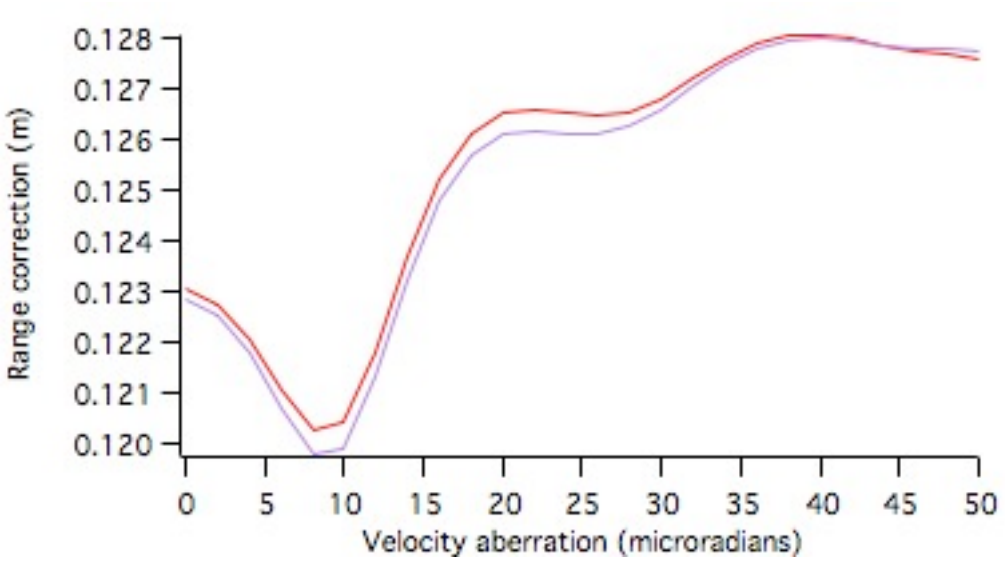

Figure 10.10. Comparison between 1.5 arcsec (red) and actual dihedral angles (purple) of the range correction vs velocity aberration over 1080 orientations with circular polarization.

Below is an expanded version of figure 10.10

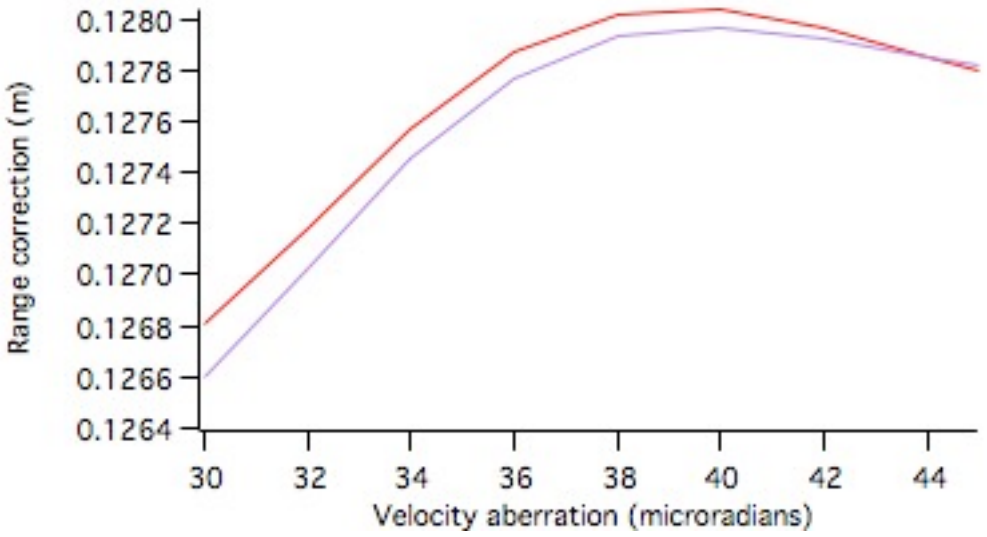

Figure 10.11. Expanded version of figure 10.10. The difference between using 1.5 arcsec (red) and the actual dihedral angle offsets (purple) is only about .2 millimeters.

The figure below is for the actual dihedral angles with linear vertical polarization.

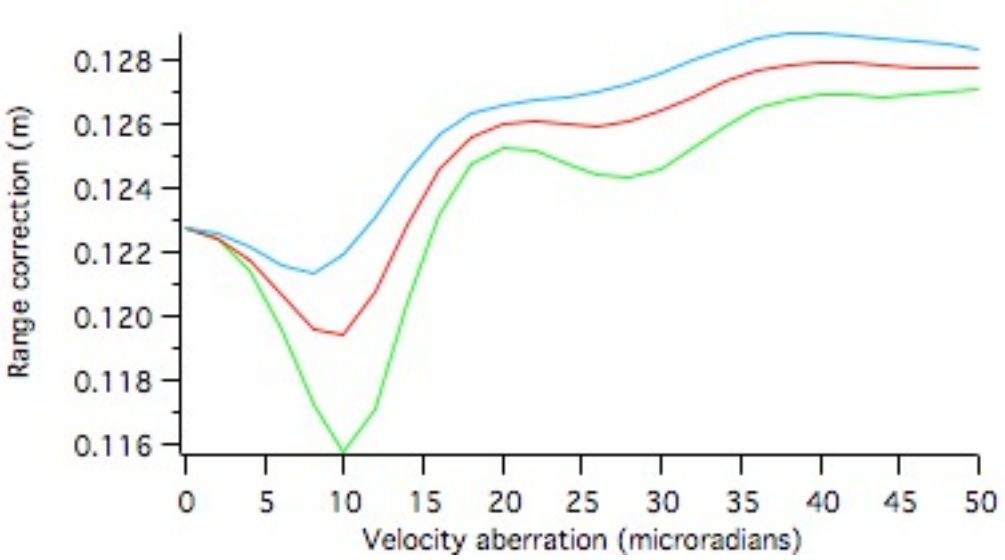

Figure 10.12. Centroid vs velocity aberration averaged over 1080 orientations with actual dihedral angles and linear vertical polarization.

Microrad	Minimum	Average	Maximum	Max - Min
0.0	0.1227500	0.1227500	0.1227500	0.0000000
2.0	0.1223791	0.1224398	0.1225800	0.0002009
4.0	0.1213656	0.1217162	0.1221300	0.0007644
6.0	0.1195868	0.1206275	0.1215900	0.0020032
8.0	0.1172500	0.1195885	0.1213600	0.0041100
10.0	0.1157600	0.1194457	0.1218612	0.0061012
12.0	0.1170700	0.1207643	0.1230901	0.0060201
14.0	0.1203700	0.1228326	0.1244942	0.0041242
16.0	0.1231700	0.1245518	0.1255960	0.0024260
18.0	0.1247000	0.1255657	0.1262685	0.0015685
20.0	0.1252200	0.1259944	0.1265895	0.0013695
22.0	0.1251200	0.1260585	0.1267137	0.0015937
24.0	0.1247200	0.1259707	0.1267964	0.0020764
26.0	0.1243600	0.1259252	0.1269343	0.0025743
28.0	0.1242900	0.1260456	0.1271900	0.0029000
30.0	0.1245900	0.1263715	0.1275600	0.0029700
32.0	0.1251900	0.1268242	0.1279600	0.0027700
34.0	0.1258700	0.1272825	0.1283300	0.0024600
36.0	0.1264300	0.1276309	0.1286100	0.0021800
38.0	0.1267546	0.1278265	0.1287500	0.0019954
40.0	0.1268653	0.1278839	0.1287900	0.0019247
42.0	0.1268549	0.1278532	0.1287400	0.0018851
44.0	0.1268333	0.1277948	0.1286500	0.0018167
46.0	0.1268625	0.1277519	0.1285487	0.0016862
48.0	0.1269549	0.1277327	0.1284390	0.0014841
50.0	0.1270725	0.1277171	0.1283196	0.0012471

Table 10.4. Data used to plot figure 10.12 with actual dihedral angle offsets and linear vertical polarization. This should be the best estimate of the range correction for linear

polarization. The range correction varies by 1.5 millimeters over the range 30 to 45 microradians.

The plot below compares circular and linear vertical polarization with actual dihedral angle offsets.

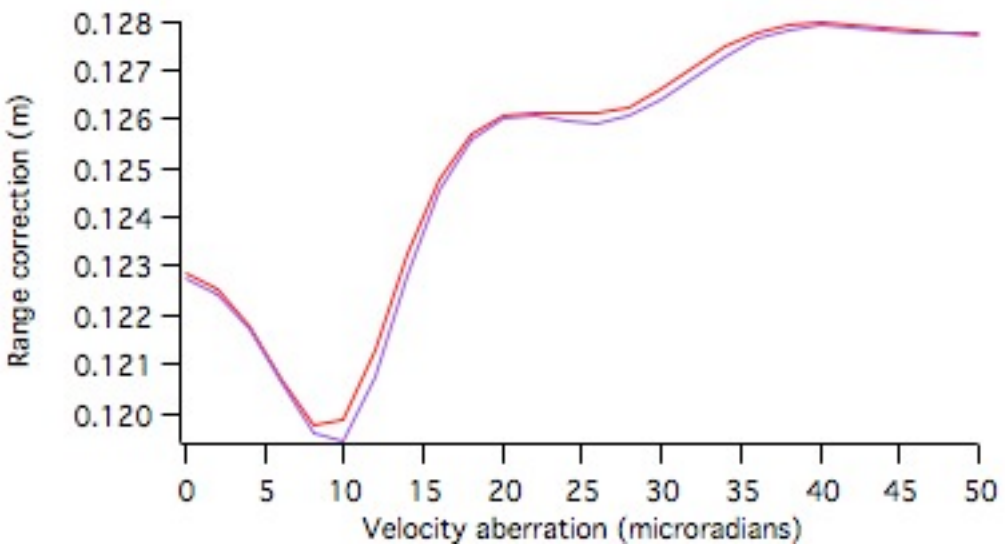

Figure 10.13. Compare circular (red) and linear vertical (purple) polarization with actual dihedral angle offsets.

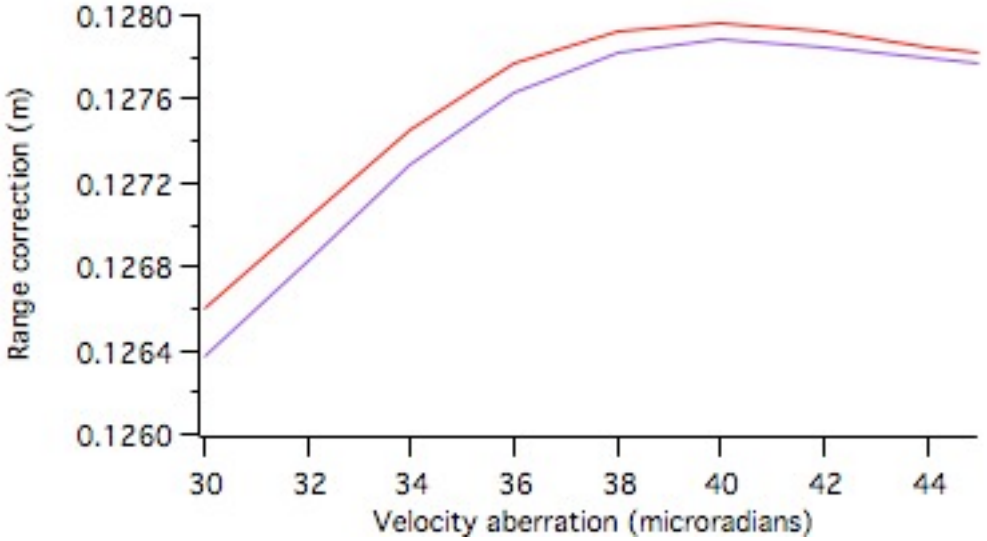

Figure 10.14. Expanded version of figure 10.13 with actual dihedral angle offsets. The difference between circular (red) and linear vertical polarization (purple) is only about .2 millimeters.

10.4. Centroid and half maximum range correction for a single point in the far field.

The receiver only sees one point the far field pattern. The graph below shows how the centroid range correction varies at a single point in the far field pattern as the incidence angles spirals from colatitude 15 deg to the equator at colatitude 90 deg.

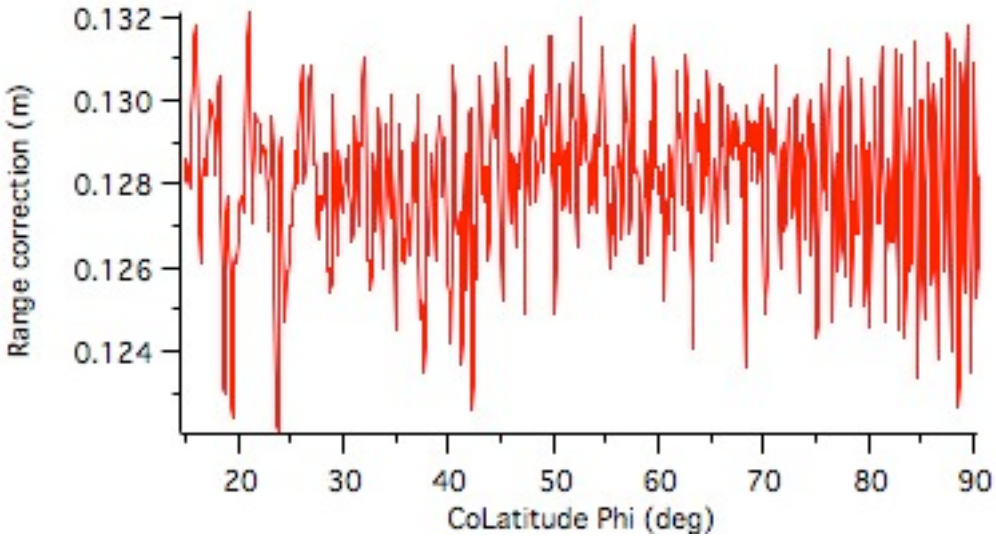

Figure 10.15. Centroid range correction vs colatitude at velocity aberration (36,0). The minimum is .1221m, the maximum is .1321m, max – min = .0100m, the average is .12808m, and the r.m.s. variation is .0017m (1.7 mm). The dihedral angle offset is 1.5 arcsec and the polarization is circular.

The graph below shows how the half maximum range correction varies at velocity aberration (36,0) as the incidence angle spirals from colatitude 15 deg to 90 deg (equator).

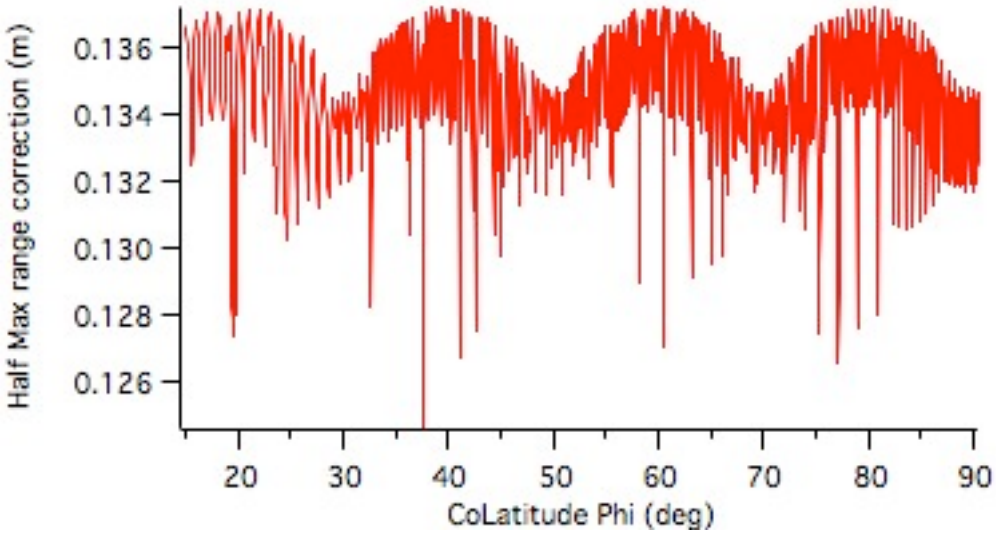

Figure 10.16. Half maximum range correction vs colatitude at velocity aberration (36,0). The half maximum range depends on the transmitted pulse width which is 30 picoseconds. The minimum is .1246 m, the maximum is .1372 m, max – min = .0126 m, the average is .1346 m, and the r.m.s. variation is .0018 m (1.8 mm). There is clearly a systematic variation with colatitude. The graph below shows an expanded plot of the top part of the graph.

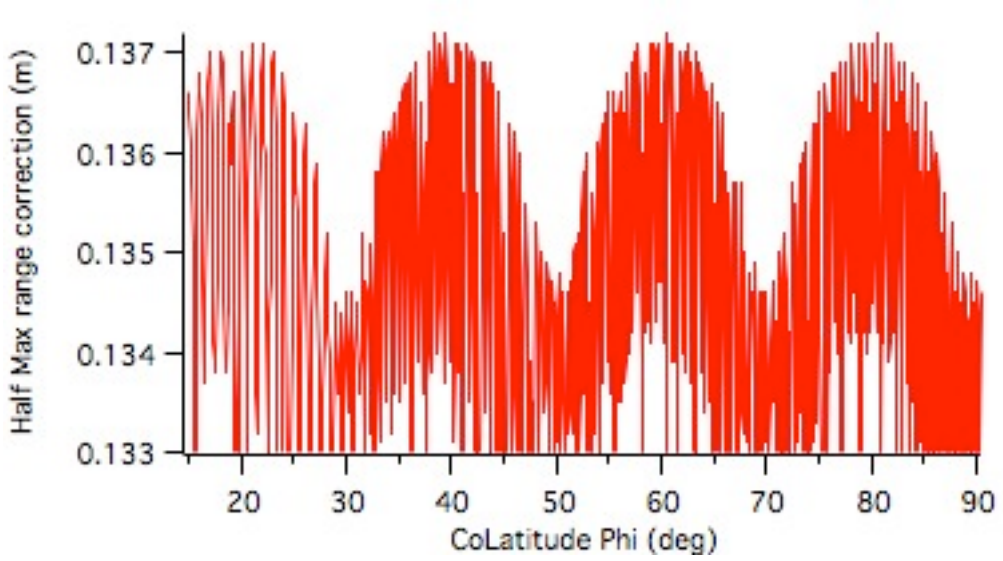

Figure 10.17. Expanded plot of Figure 10.16 showing the details of the structure of the pattern.

The upper envelope of the plot shows peaks at 20, 40, 60, and 80 deg colatitude. These are the locations of the rings of cubes. The apparent reflection point when the incidence angle is normal to a cube corner is r = 135 mm which include the recession and the optical path length in the cube corner. When the angle of incidence is between two rows the position z of the apparent reflection point along the line of sight of the closest cube corner is approximately

$$z = r\cos(10\,\text{deg}) \qquad (10.1)$$

From equation (10.1) we have z = 132.95. The difference in range is 135 – 132.95 = 2.05 mm. This agrees approximately with the difference between the peaks and valleys in figure 10.17.

The behavior seen in figure 10.17 should also occur if the incidence angle is going along a ring of cube corners since the spacing between cubes in a ring is about the same as the spacing between rings. Starting at the North pole the first three rings have 1, 5, and 10 cube corners. Table 3.4 gives the longitude and colatitude of each cube. The colatitude of the third ring is 40 deg. A simulation has been done with the longitude starting at 0 and incrementing one deg between points. The colatitude is constant at 40 deg. There are 361

points which is once around the satellite. The figure below shows the centroid range correction vs longitude.

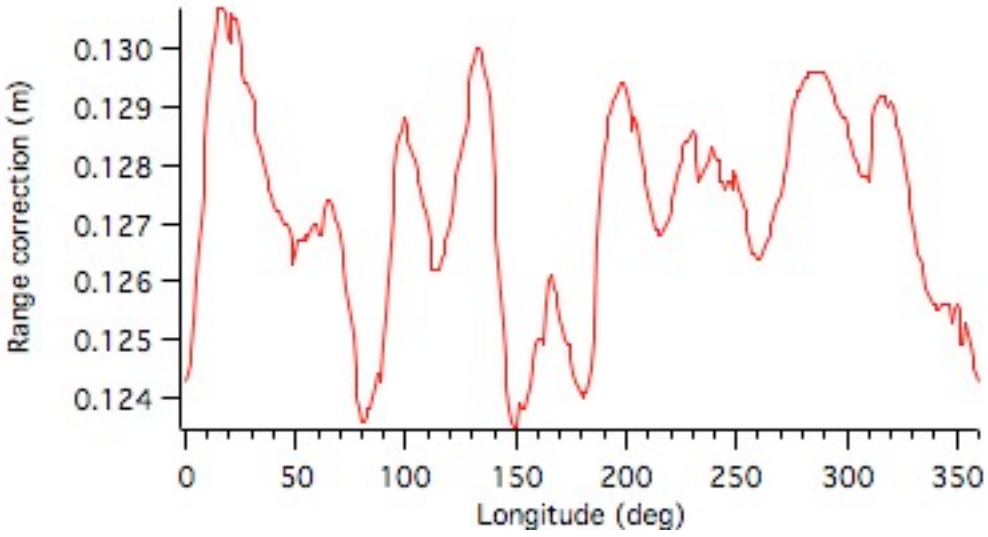

Figure 10.18. Centroid range correction vs longitude at velocity aberration (36,0) with dihedral angle 1.5 arcsec and circular polarization. The colatitude is 40 deg. The minimum is .12355 m, the maximum .1307 m, max – min .00715 m, average .1272 m, and the r.m.s. variation .00177m (1.77mm).

The figure below shows the half maximum range correction for the same case as figure 10.18.

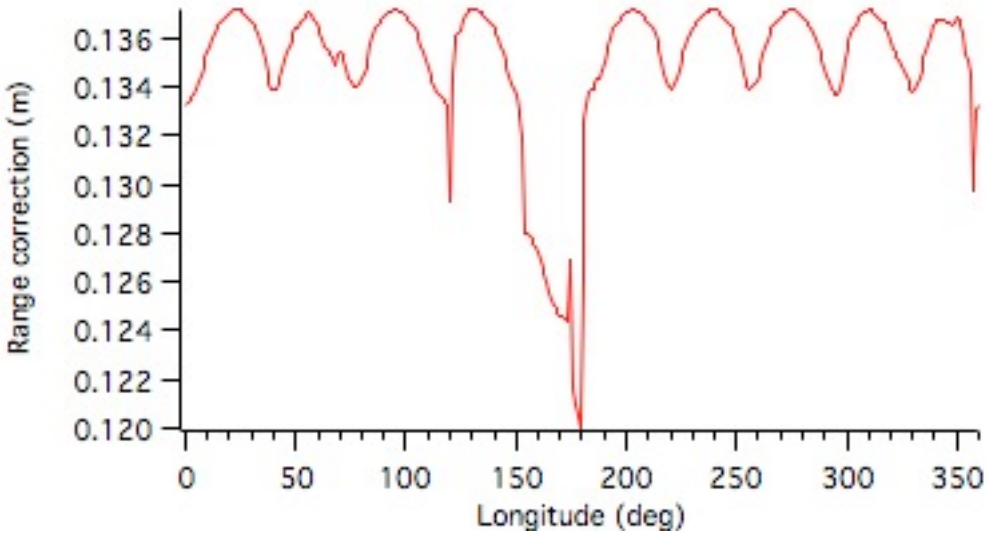

Figure 10.19. Half maximum range correction for the same case as figure 10.18. The minimum is .1200 m, maximum .1372 m, max – min .0172 m, the average is.1349 m, and

r.m.s. variation .003 m (3 mm). The figure below shows an expanded version of the top of the graph.

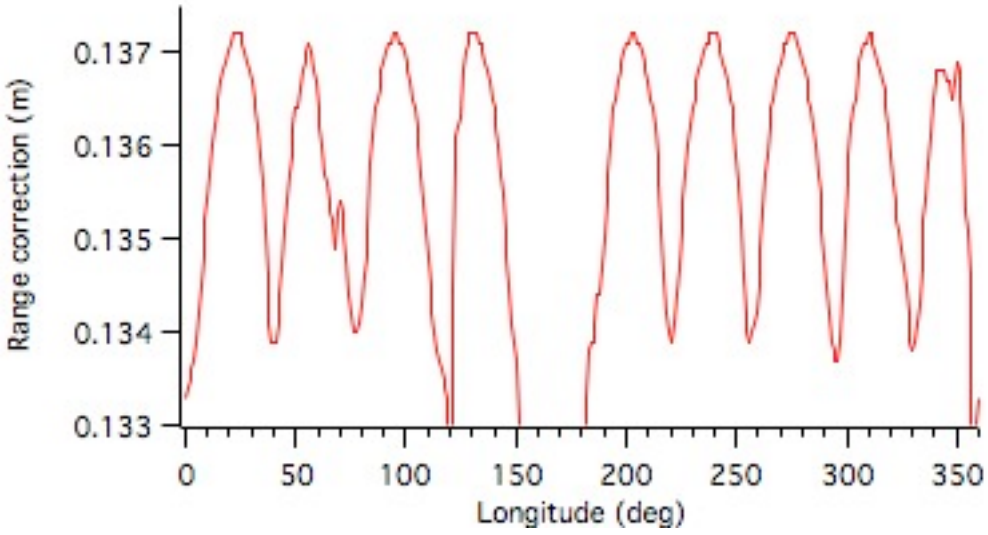

Figure 10.20. Expanded version of the top of figure 10.19. The range varies from about .134 to .137 m, an amplitude of about 3 mm over most of the graph.

Figure 10.19 shows anomalous behavior at 179 longitude. This is due to an irregular pulse shape shown below.

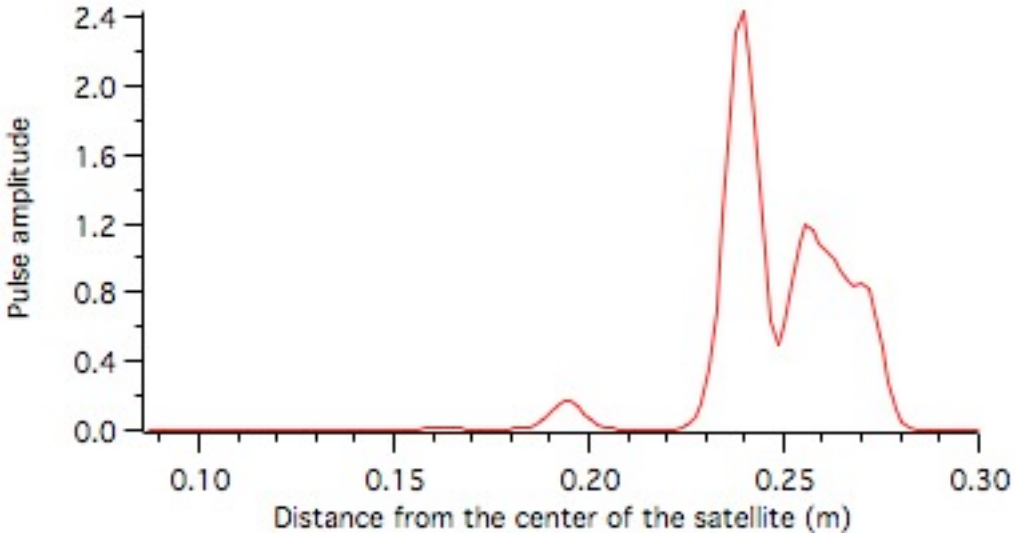

Figure 10.21. Pulse shape at longitude 179 deg, colatitude 40 deg for the case of figure 10.19. The reason for the anomalous half maximum range correction is that the first peak is not quite half as high as the highest peak. This kind of anomalous behavior occurs in figure 10.16 also.

10.5 Summary of section 10.

The range correction matrix at a single incidence angle has an irregular shape for both circular and linear polarization. However, when matrices over many incidence angles are averaged a regular pattern emerges. For circular polarization the pattern becomes circular. The range correction is a function of the magnitude of the velocity aberration but does not vary much around a circle in the far field. For linear vertical polarization the pattern has left to right symmetry. There is a variation around a circle with a peak to peak variation of up to 3 mm. The asymmetry is greatest for low velocity aberration. The range correction as a function of velocity aberration is almost identical for circular and linear polarization.

The specification on the dihedral angle is 90 + 1.5 +/- 0.5 arcsec. The angle can vary between 1.00 and 2.00 arcsec. The average range correction can vary up to 2 mm over this range of dihedral angle offset.

The dihedral angles of all the cube corners have been measured. The average value is 1.58 arcsec. Simulations with the actual dihedral angle offsets give results that are almost identical to using 1.50 arcsec for all cube corners. The centroid range correction for both circular and linear polarization is repeated below for the range 30 to 45 microradians.

Microrad	Circular(m)	Linear(m)
30.0	0.1265930	0.1263715
32.0	0.1270283	0.1268242
34.0	0.1274531	0.1272825
36.0	0.1277645	0.1276309
38.0	0.1279288	0.1278265
40.0	0.1279638	0.1278839
42.0	0.1279181	0.1278532
44.0	0.1278470	0.1277948
46.0	0.1277905	0.1277519

Table 10.5. Range correction vs velocity aberration for circular and linear polarization with the actual dihedral angle offsets.

The average range correction for linear polarization in Table 10.5 over the range from 30 to 45 microradians is 127.4 mm. This should be the best estimate for actual ranging data.

Simulations have been done to calculate the centroid and half maximum range correction over many incidence angles at a single point in the far field with velocity aberration components (36,0) microradians. The centroid shows an average value of .128 m with an r.m.s variation of 1.7 mm. There do not seem to be any clear systematic effects. The half maximum range correction with a 30 ps transmitted pulse shows an average value of .1346 m with an r.m.s. variation of 1.8 mm. There is a clear systematic effect depending on whether the incidence angle is directly over a cube corner or between cube corners. The peak to peak variation is 2 or 3 millimeters. The half maximum correction can give anomalous results if the return pulse has multiple peaks the the first peak is less than half the highest peak.

11. Effect of optical coherence.

All the calculations done previously in this report are for the incoherent case. The signal is computed as the sum of the energy from each cube corner. Since the laser beam is coherent there will be interference among the returns from different cube corners. One can think of coherent interference as computing the diffraction pattern of the whole array which has multiple apertures. When the diffraction pattern of an array is measured there is speckling of the pattern due to the interference between the returns from different cube corners. In the laboratory the array can be vibrated to vary the phases between the cubes and produce the incoherent diffraction pattern with a time exposure.

There are many factors that affect coherent interference:

1. Coherent interference depends on the pulse length and distance between cube corners along the line of sight.
2. The distribution of retroreflectors along the line of sight is different for every incidence angle.
3. The signal from each cube corner is different at each point in the far field pattern
4. The far field pattern is different for circular and linear polarization.
5. The pattern depends on the angle of linear polarization.
6. Coherent interference occurs separately for the x and y polarization components.
7. The transmitted pulse is not strictly monochromatic since the pulse is of finite length.

In order to try to make the results more representative of the average behavior an incidence angle has been selected that has close to the average cross section and centroid range correction between 30 and 45 microradians. The average cross section (sum of both polarization components) between 30 and 45 microradians has been used as the signal from each cube corner for computing the coherent interference. Ignoring factors 6 and 7 probably results in overestimating the variations due to coherent interference. The method of computing the coherent return is described in section 7.8 of reference 1, “Method of calculating Retroreflector array transfer functions. A random number generator is used to assign random phases to each cube corner for each coherent return.

There are a large number of transmitted pulse lengths that have been used, such as 10, 20, 30, 35, 40, 50, 60, 70, 100, 130, 150, 190, 200, 250, 300, 350, 2500, 3000, and 5000 ps. Of these the most common are 10, 35, 100, 200, and 300. It turns out that the effects of coherence vary continuously with transmitted pulse length. In order to see the overall picture the pulse lengths that have been used in this analysis are 5, 10, 20, 30, 100, 200, 300, 1000, 3000, and 10000 ps. This covers the range from pulse lengths short compared to the size of the array to pulse lengths long compared to the size of the array.

From simulations that have been done over most of the satellite an incidence angle of Longitude 185 deg and colatitude 107.71 has been chosen. This incidence angle has very close to the average cross section and range correction. The distribution of cube corners is reasonably similar to the average histogram of the satellite shown in figure 8.1. The

figure below shows the active cube corners for this incidence angle superimposed over the average histogram of figure 8.1.

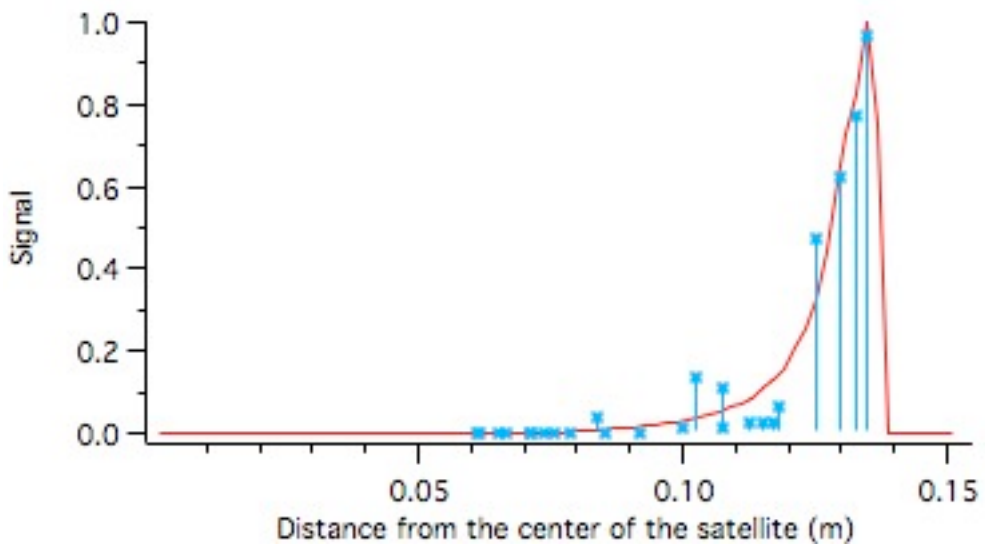

Figure11.1. Distribution of the active cube corners (blue with markers) superimposed on the average pulse histogram over many incidence angles. The strength of the return of the points in blue is the average cross section over the 30 to 45 microradian annulus in the far field. The signal is in normalized units.

In order to determine the variation of the transfer function a set of 9999 coherent returns have been computed for the distribution of cube corners shown in figure 11.1 for transmitted pulse lengths 5, 10, 20, 30, 100, 200, 300, 1000, 3000, and 10000 ps. Three pulse length, 10, 100, and 10,000 ps have been studied in detail to show how coherent interference depends on pulse length. The quantities studies are the cross section, centroid range correction and half maximum range correction (the half maximum point on the leading edge). Histograms of the cross section, centroid, and half max range correction have been computed. The cross section is in bins of .5 million sq m. The range is in bins of 1 mm.

The figures below show histograms for transmitted pulse lengths of 10, 100, and 10,000 ps. The graphs have been condensed to allow comparison of the results for different pulse lengths. This makes the axes hard to read without expanding the scale. The vertical axis is the probability distribution normalized to a maximum value of unity, the horizontal axis is million sq meters for the cross section, and meters for the range. The cross section is plotted from 0 to 14 million sq m for the 10 and 100 ps pulse lengths. The range is plotted from 0 to .15 m. For the 10,000 ps pulse length the cross section is plotted from 0 to 20 million sq m. The range is plotted from 0 to .20 meters.

Pulse length 10 ps.

Cross section Centroid Half max

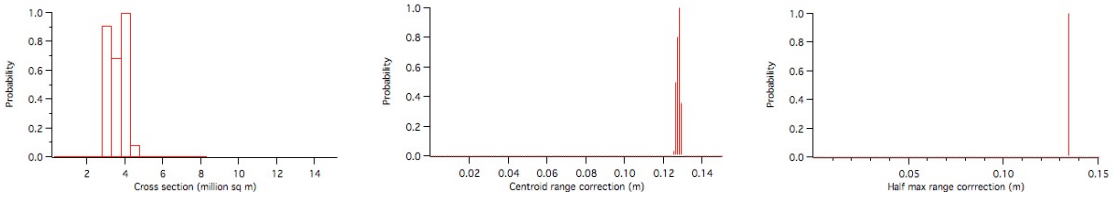

(a) (b) (c)

Figure 11.2 Histograms of the cross section (a), centroid (b), and half max range correction (c) for transmitted pulse length 10 ps.

Pulse length 100 ps.

Cross section Centroid Half max

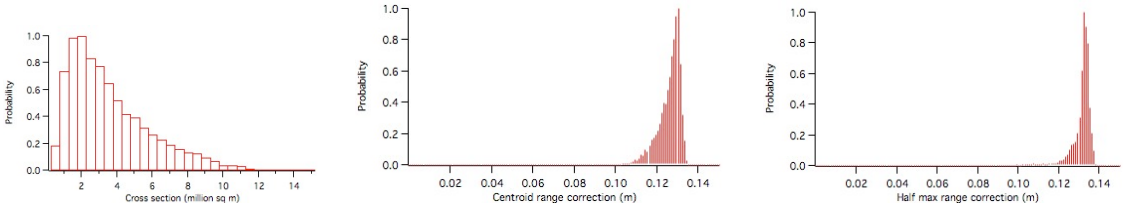

(a) (b) (c)

Figure 11.3 Histograms of the cross section (a), centroid (b), and half max range correction (c) for transmitted pulse length 100 ps.

Pulse length 10,000 ps.

Cross section Centroid Half max

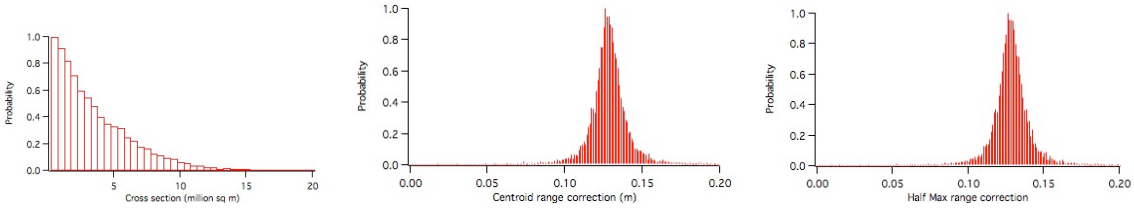

Figure 11.4 Histograms of the cross section (a), centroid (b), and half max range correction (c) for transmitted pulse length 10,000 ps.

The figures below show the r.m.s. variation of cross section, centroid, and half max range correction vs pulse length. The plots are shown at full scale so that the axes are readable.

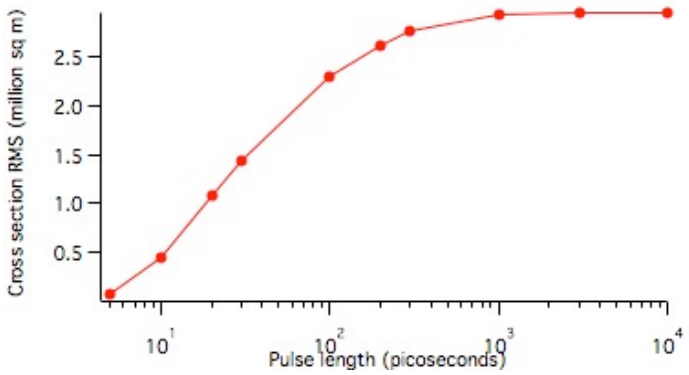

Figure 11.5. r.m.s. variation of the cross section vs transmitted pulse length (log scale) for pulse lengths 5, 10, 20, 30, 100, 200, 300, 1000, 3000, and 10000 ps.

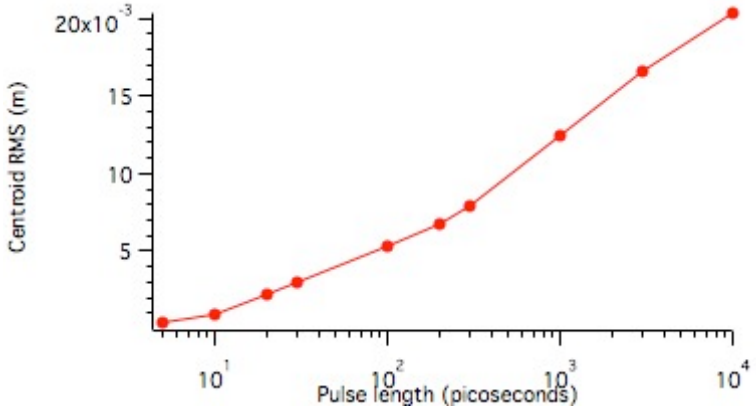

Figure 11.6. r.m.s. variation of the centroid vs transmitted pulse length (log scale) for pulse lengths 5, 10, 20, 30, 100, 200, 300, 1000, 3000, and 10000 ps.

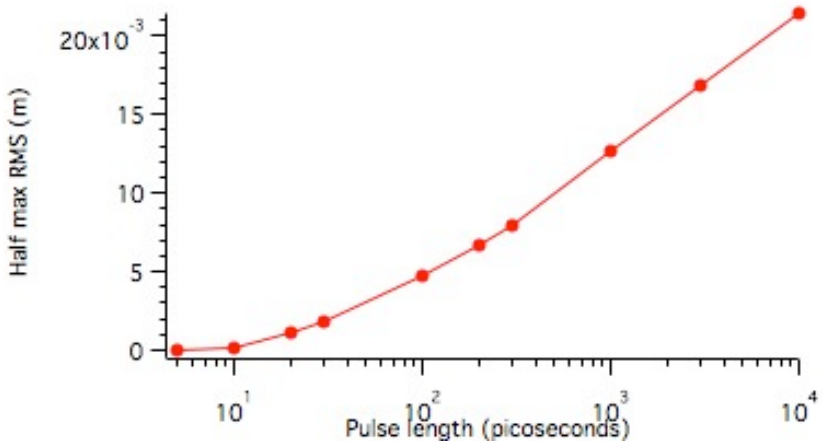

Figure 11.7. r.m.s. variation of the half max range correction vs transmitted pulse length (log scale) for pulse lengths 5, 10, 20, 30, 100, 200, 300, 1000, 3000, and 10000 ps.

The figures below show the average value of cross section, centroid, and half max range correction vs pulse length.

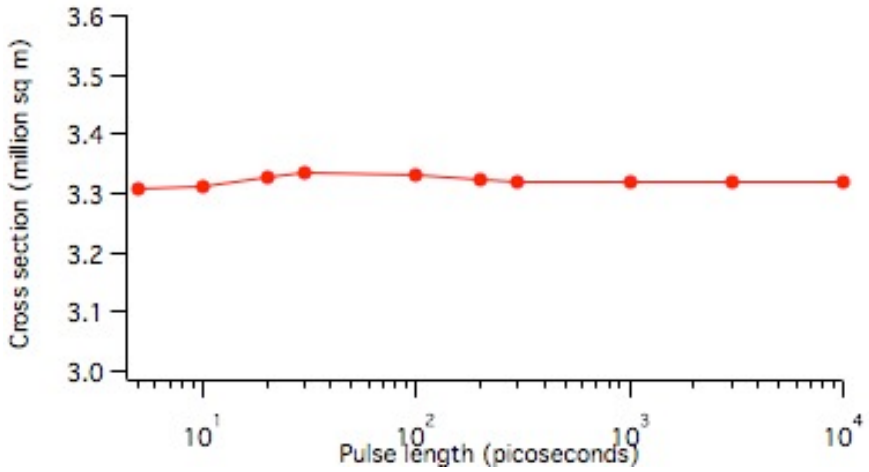

Figure 11.8. Average value of the cross section for 9999 coherent return vs pulse length. The average value is almost constant and varies between 3.308 and 3.335 million sq m.

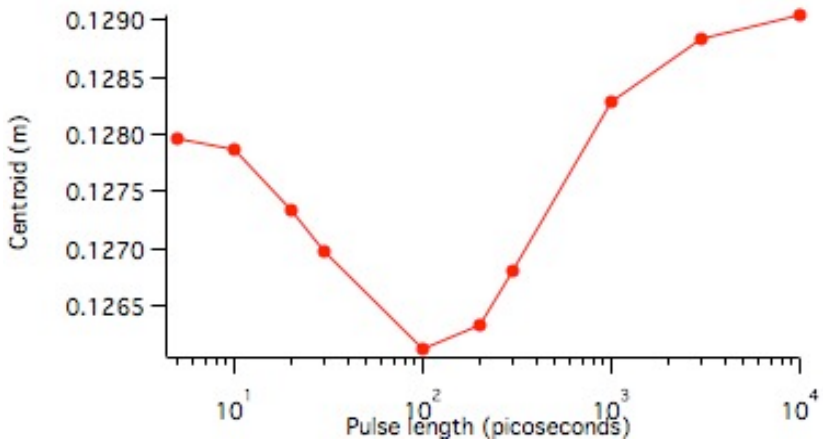

Figure 11.9. Average value of the centroid for 9999 coherent return vs pulse length.

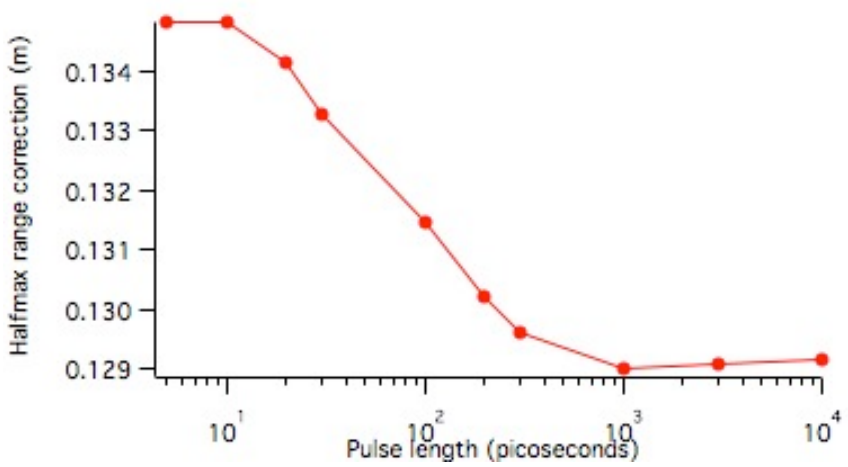

Figure 11.10. Average value of the half max range correction vs pulse length.

The figures below compare the average centroid and half max range correction with equal weighting of the coherent returns and weighted by signal strength.
Red = centroid
Green = halfmax

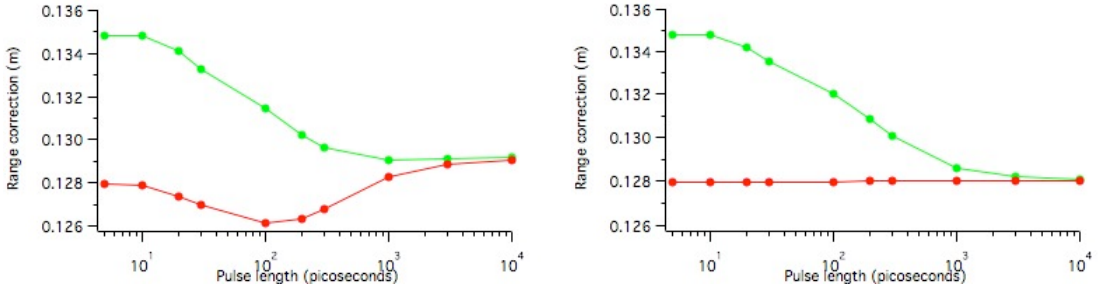

Equal weighting (a) Weighted by signal strength (b)

Figure 11.11. Comparison of average over 9999 coherent returns of the centroid (red) and half max range correction (green) with equal weighting (a) and weighted by signal strength (b). Equal weighting removes the variation in the centroid for all pulse lengths and removes the bias in the half max range correction above 10,000 ps.

The figures below show the difference between the incoherent return and the average coherent return with equal weighting and weighted by signal strength.

Equal weighting

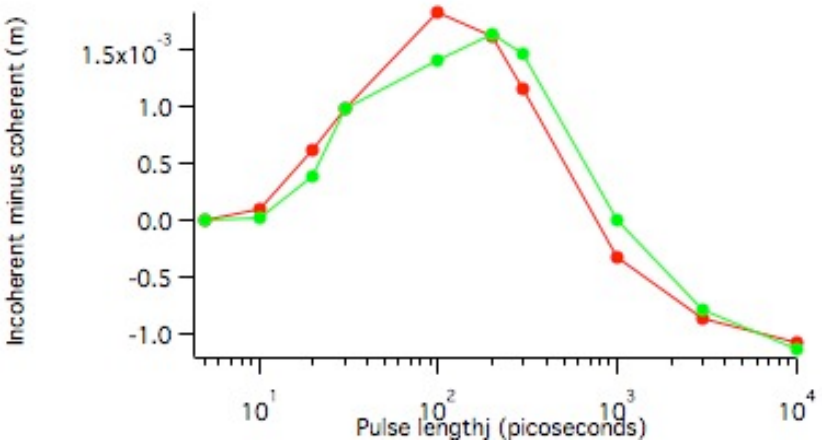

Red = centroid
Green = halfmax

Figure 11.12. Difference between the incoherent return and the average coherent return vs pulse length with equal weighting. There is not much difference.

Weighted by signal strength

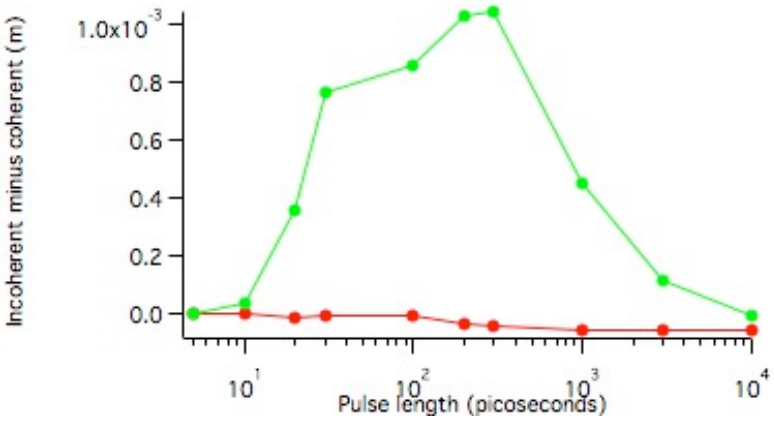

Red = centroid
Green = halfmax

Figure 11.13. Difference between the incoherent return and the average coherent return vs pulse length weighted by signal strength. Equal weighting removes the bias in the centroid for all pulse length and the bias in the half max range correction above 10,000 ps pulse length

Summary of results

Coherent interference is disappearing below 5 picoseconds pulse length. The difference between centroid and half max range correction disappears above 10,000 picoseconds. The average coherent cross section is the same as the incoherent cross section. The probability distribution of the cross section becomes exponential for pulse lengths long compared to the size of the array. The average coherent range correction for both centroid and half max is not the same as the incoherent range correction for pulse lengths between 5 and 10,000 picoseconds. Weighting the returns by signal strength removes the bias in the centroid range correction for all pulse lengths. Weighting by signal strength removes the bias in the half max range correction only above 10,000 picoseconds pulse length. Since the signal strength is always the same for single photoelectron systems there is automatic weighting by signal strength and no bias in the centroid due to coherent interference. The coherent pulse shape is the probability function for getting a photoelectron. This is governed by Poisson statistics. Photon quantization can be modeled in the program but has not been studied in this report.

12. Accuracy of the results.

The current goal for the accuracy of a retroreflector array is 1 mm. In Table 10.5 the centroid range correction for linear polarization varies from a minimum of 0.1263715 m at 30 microradians to a maximum of 0.1278839 m at 40 microradians. This is a difference of 1.5 mm. Since the velocity aberration is known a correction for this could be applied during analysis. If a constant correction is used there would be a maximum error of .75 mm. This meets the requirement. The difference between linear and circular polarization in Table 10.5 is .2 mm. This meets the accuracy requirement. In Figure 10.14 the difference in range between using the actual dihedral angles and the nominal dihedral angle offset of 1.5 arcsec is .2 mm. This meets the accuracy requirement. In table 10.2 the variation around a circle at 30 microradians in the far field with linear polarization has a peak to peak variation of 3 mm. If this is neglected there is a maximum error of 1.5 mm which exceeds the accuracy requirement. The correction depends on the angle between the transmitted polarization and the direction of the velocity aberration. If these quantities are known a correction could be applied during analysis. If the angle between the polarization vector and the velocity aberration varies randomly the error will average out. In Table 10.1 which gives the average range correction matrix for circular polarization the largest difference around a circle in the far field is .9 mm at 45 microradians. The variations around a circle do not average out completely however the remaining variations are within the accuracy requirement and a factor of 3 less than for linear polarization. Figure 10.15 shows the variation of the centroid range correction over many incidence angles at a single point in the far field. The dihedral angle offset is 1.5 arcsec and the polarization is circular. The peak to peak variation of the range is 10 mm. The average is 128.08 mm. The r.m.s. variation is 1.7 mm. Since the variations are random they should average out over many observations. The dihedral angle offset can vary from 1.0 to 2.0 arcsec within the specified tolerance of 1.5 +/- 0.5 arcsec. Figures 10.7 and 10.8 show the variation of the average range correction matrix vs dihedral angle offset. There can be significant variations if the dihedral angle offset were not correct. However,

the actual dihedral angles as shown in figure 2.1 have an average value of 1.58 arcsec. So this can be ruled out as a possible source of error.

There are many unmodeled effects in the simulation program such as thermal gradients, variations in surface flatness, variations in index of refraction of the material, etc. The contribution of these effects is not known. The range errors due to the parameters modeled in the program do not show any systematic errors that are outside the 1 mm accuracy goal. The best estimate of the centroid range correction as a function of the magnitude of the velocity aberration is given in Table 10.5.

14. References

1. I. Ciufolini, A. Paolozzi, E. Pavlis, J. Ries, R. Koenig, R. Matzner, G. Sindoni. The LARES Space Experiment: LARES Orbit, Error Analysis and Satellite Structure. In: General Relativity and John Archibald Wheeler. I. Ciufolini and R. Matzner eds., 467-492 (Springer, 2010).
2. I. Ciufolini, A. Paolozzi, C. Paris. Overview of the LARES Mission: orbit, error analysis and technological aspects. Journal of Physics, Conference Series, vol. 354, p. 1-9. 2012.
3. A. Paolozzi, I. Ciufolini, E. Flamini, A. Gabrielli, S. Pirrotta, E. Mangraviti, A. Bursi. LARES in orbit: Some aspects of the mission. Proceedings of the International Astronautical Congress, IAC, Volume 6, 2012, Pages 4468-4474. 63rd International Astronautical Congress 2012, IAC 2012; Naples; Italy; 1 October 2012 through 5 October 2012; Code 98825.
4. Paolozzi, I. Ciufolini. LARES successfully launched in orbit: satellite and mission description. Acta Astronautica, Volume 91, October–November 2013, Pages 313–321.
5. I. Ciufolini, D. G. Currie, A. Paolozzi. The LARES mission for testing the dynamics of general relativity. Aerospace Conference, 2003. Proceedings. 2003 IEEE. Volume: 2, pp. 693-703.
6. I. Ciufolini, A. Paolozzi, R. König, E. C. Pavlis, J. Ries, R. Matzner, V. Gurzadyan, R. Penrose, G. Sindoni, C. Paris (2013). Fundamental Physics and General Relativity with the LARES and LAGEOS satellites. Nuclear Physics B - Proceedings Supplements, 243-244, 180-193.
7. I. Ciufolini, A. Paolozzi, E. C. Pavlis, J. C. Ries, R. Koenig, R. A. Matzner, G. Sindoni, H. Neumayer. Towards a One Percent Measurement of Frame Dragging by Spin with Satellite Laser Ranging to LAGEOS, LAGEOS 2 and LARES and GRACE Gravity Models. Space Science Reviews, December 2009, Volume 148, Issue 1-4, pp 71-104.
8. A. Paolozzi, I. Ciufolini, A. Lucantoni, D. Arnold (2009). Optical Design of LARES Satellite. Proceedings of XX AIDAA Congress. Milano, Italy, June 29-July 3, 2009.
9. A. Paolozzi, I. Ciufolini, L. Schirone, I. Peroni, C. Paris, D. Spano, G. Sindoni, C. Vendittozzi, G. Battaglia, M. Ramiconi. Tests of LARES Cube Corner Reflectors in

Simulated Space Environment (preliminary results). 61st International Astronautical Congress, Prague, CZ, 27 September – 1 October 2010.
10. A. Paolozzi, I. Ciufolini, C. Paris, G. Sindoni, D. Spano. Qualification tests on the optical retro-reflectors of LARES satellite. Proceedings of 63rd International Astronautical Congress. Naples, Italy, 1-5 October, 2012. IAC 8 , pp. 6280-6286.
11. A. Paolozzi, I. Ciufolini, F. Felli, A. Brotzu, D. Pilone. Issues on LARES satellite material. 60th International Astronautical Congress, IAC 2009; Daejeon, Korea; 12-16 October 2009.
12. A. Paolozzi, I. Ciufolini, C. Vendittozzi, F. Passeggio, L. Caputo, G. Caputo. Technological challenges for manufacturing LARES satellite. 60th International Astronautical Congress, IAC 2009; 12-16 October 2009.
13. A. Paolozzi, I. Ciufolini, C. Vendittozzi, F. Felli. Material and surface properties of LARES satellite (conference paper). Proceedings of the International Astronautical Congress, IAC. Volume 8, 2012, Pages 6559-6565. 63rd International Astronautical Congress 2012, IAC 2012; Naples; Italy; 1 October 2012 through 5 October 2012; Code 98825
14. A. Paolozzi, I. Ciufolini, C. Vendittozzi. Engineering and scientific aspects of LARES satellite. ACTA ASTRONAUTICA, 69:127–134, 2011.
15. I. Ciufolini, A. Paolozzi, G. Sindoni and C. Paris. LARES Satellite: the best test particle for testing General Relativity. Proceedings of XXII AIDAA Conference, Neaples (Italy), September 9th - 12th, 2013
16. A. Paolozzi, I. Ciufolini, C. Vendittozzi, I. Peroni,, Mechanical Design of LARES Satellite, Proceedings of XX AIDAA Congress. Milano, Italy, June 29-July 3, 2009.
17. D.A. Arnold Method of Computing Retroreflector Array Transfer Functions, SAO Special Report 382. http://ilrs.gsfc.nasa.gov/about/reports/other_publications.html.